iScience

CellPress
OPEN ACCESS

Article

REC domain stabilizes the active heptamer of σ^{54}-dependent transcription factor, FleR from *Pseudomonas aeruginosa*

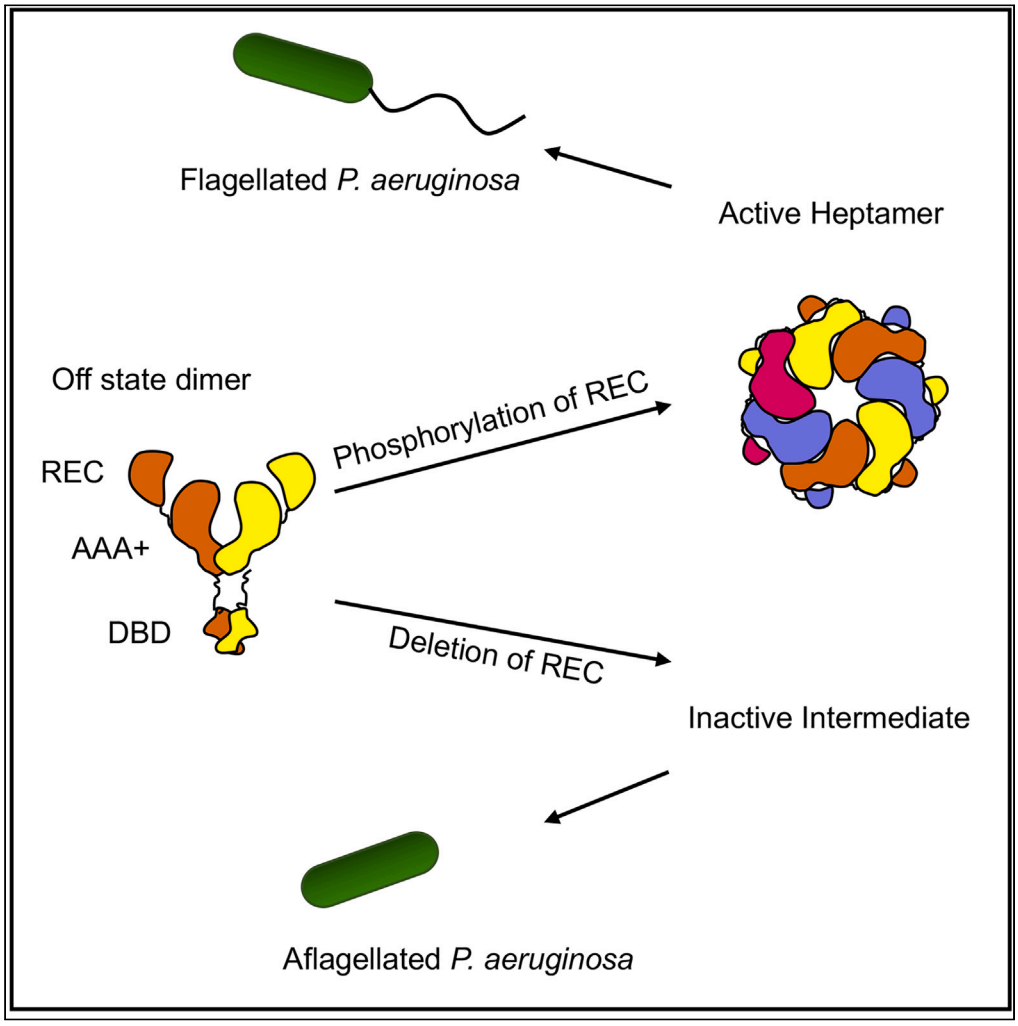

Pankaj Kumar Sahoo, Sheenu, Deepti Jain

deepti@rcb.res.in

Highlights

Structure of flagellar regulator FleR in active and inactive states is reported

SAXS structure of non-phosphorylated form reveals a dimer with low ATPase activity

Negative staining EM of phosphorylated FleR shows heptamer stabilized through REC domain

Deletion of REC domain results in aflagellate phenotype of *P. aeruginosa*

Sahoo et al., iScience *26*, 108397
December 15, 2023
https://doi.org/10.1016/j.isci.2023.108397

iScience

CellPress
OPEN ACCESS

Article

REC domain stabilizes the active heptamer of σ^{54}-dependent transcription factor, FleR from *Pseudomonas aeruginosa*

Pankaj Kumar Sahoo,[1] Sheenu,[1] and Deepti Jain[1,2,*]

SUMMARY

Motility in *Pseudomonas aeruginosa* is mediated through a single, polar flagellum, which is essential for virulence, colonization, and biofilm formation. FleSR, a two-component system (TCS), serves as a critical checkpoint in flagellar assembly. FleR is a σ^{54}-dependent response regulator that undergoes phosphorylation via cognate sensor kinase FleS for the assembly of the functionally active form. The active form remodels the σ^{54}-RNAP complex to initiate transcription. Small-angle X-ray scattering, crystallography, and negative staining electron microscopy reconstructions of FleR revealed that it exists predominantly as a dimer in the inactive form with low ATPase activity and assembles into heptamers upon phosphorylation with amplified ATPase activity. We establish that receiver (REC) domain stabilizes the heptamers and is indispensable for assembly of the functional phosphorylated form of FleR. The structural, biochemical, and *in vivo* complementation assays provide details of the phosphorylation-mediated assembly of FleR to regulate the expression of flagellar genes.

INTRODUCTION

σ^{54} is a unique sigma factor that, upon interaction with core RNA polymerase (RNAP), recognizes the promoters of genes associated with diverse functions such as flagellar biosynthesis, pilin synthesis, quorum sensing, nitrogen assimilation, and response to phage infections.[1–5] σ^{54}-dependent promoters have conserved consensus sequences at the −12 and −24 positions upstream of the transcription start site. However, σ^{54}-RNAP is incapable of melting double-stranded DNA to initiate transcription and requires the energy derived from ATP hydrolysis by a transcription activator to form an open promoter complex. ATP hydrolysis is stimulated upon oligomerization of the activator and is a prerequisite for transcription activation. The activators usually bind to DNA far upstream of the transcription start site, analogous to eukaryotic enhancer-binding proteins (EBP). σ^{54}-dependent transcription activators are thus referred to as bacterial EBPs (bEBP).[6,7]

Bacterial EBPs possess a modular architecture, typically comprising three domains. These include regulatory domain at the N-terminus responsible for signal perception, a central AAA+ ATPase domain that hydrolyses ATP, and an enhancer-binding domain with a helix-turn-helix motif located at the C-terminus. Although the AAA+ domain is conserved, some members of this protein family may lack either the receiver- or enhancer-binding domain. Furthermore, these activators feature diverse sensory domains at their N-terminus, which can either positively or negatively regulate σ^{54}-dependent transcription activation. Some of the structurally well-characterized bEBP include NtrC (nitrogen regulatory protein C), NtrC1, NtrC4, ZraR (Zn^{2+}-responsive protein), FlrC (flagellar regulatory protein C), and PspF.[8–13]

FleR is a σ^{54}-dependent bEBP and is also part of the two-component system (TCS) FleSR, in *Pseudomonas aeruginosa*.[14] TCS are protein pairs that link environmental or cellular signals to changes in gene expression in the bacterium.[15] Classically, TCS consists of a histidine kinase (HK) and a response regulator (RR). While FleS is a soluble kinase, FleR is the cognate response regulator, and together they regulate flagellar motility in *P. aeruginosa*.[16] The assembly of functional flagella requires coordinated expression of approximately 50 different genes, in a cascade-like fashion with tight regulation at every level, assisted by dedicated transcription factors.[17] In bacteria with single polar flagella, such as *Pseudomonas,* FleQ occupies the top of the hierarchy that controls the expression of class II genes in σ^{54}-dependent manner.[18] The ATPase activity of FleQ is regulated via protein-protein interaction with FleN.[5,19,20] Class III genes, responsible for the formation of the flagellar hook and rod, fall under the control of FleSR.[17,21,22] Homologs of FleSR have been identified in other flagellated bacteria such as *Vibrio cholera* (FlrBC), *Shewanella oneidensis* (FlrBC), *Campylobacter jejuni* (FlgSR), and *Helicobacter pylori* (FlgSR).[23–27] Mutants of *fleS* or *fleR* are non-motile and significantly less virulent in *P. aeruginosa*.[14,28]

The signal transduction cascade through FleSR begins with FleS sensing an unidentified signal and operating as the phosphodonor. Subsequently, the receiver domain (REC) of the multi-domain response regulator FleR becomes phosphorylated, initiating the assembly of the functional oligomeric form.[21] Activated FleR is then thought to interact with the σ^{54} to mediate transcription of target genes. However, the

[1]Transcription Regulation Lab, Regional Centre for Biotechnology, NCR Biotech Science Cluster, 3rd Milestone, Faridabad-Gurgaon Expressway, Faridabad 121001, India
[2]Lead contact
*Correspondence: deepti@rcb.res.in
https://doi.org/10.1016/j.isci.2023.108397

precise nature of the conformational changes, the stoichiometry of the oligomeric assembly, and the role of the N-terminus domain in transcription regulation, if positive or negative, remain to be elucidated for FleR.

We have performed structural analysis of FleR and its constructs using small-angle X-ray scattering, X-ray crystallography, and negative staining electron microscopy. Our study reveals that FleR exists as a dimer in its non-phosphorylated form and harbors a low level of ATPase activity. Furthermore, upon phosphorylation, it assembles into symmetric heptamers with augmented ATPase activity. Deletion of REC domain results in non-functional FleR *in vivo*, establishing that the AAA+ domain is inherently incapable of functional assembly without the assistance from REC domain. Additionally, substitution at the interaction interface between REC and AAA+ domains lead to motility defects and an aflagellate phenotype in *in vivo* complementation assays. In summary, our findings suggest that FleR is positively regulated through its receiver domain to assemble into a functional heptameric form, which is obligatory for transcription activation.

RESULTS

ATP hydrolysis by FleR

Sequence comparison of FleR with other σ^{54}-dependent activators shows that, although the REC domain is diverse, the phosphorylation site of FleR is highly conserved and is composed of residues E9, D10, D53, and K103 forming the signature D(E)DDK motif (Figure S1). The ATPase domain of the FleR is reasonably conserved and carries signature sequences for ATP binding (Walker A) and hydrolysis (Walker B). Structural studies on other bEBPs have revealed that AAA+ domain consist of two subdomains, the α/β and the α-helical. The nucleotide-binding site is present at the crevice formed between the two subdomains. The central domain also harbors sensor I and sensor II motifs that have been implicated in modulating the ATPase activity (Figure S1).[18,29] Similar to other members of this family, FleR also contains conserved Arg residue (R finger) that functions to enhance the ATPase activity of the oligomeric protein in *trans*.[30] Another conserved structural feature includes the presence of L1 loop with GAFTGA signature sequence (GSFTGA in case of FleR) and L2 loop, which engage with N-terminus of σ^{54} (Figure S1).

We cloned, expressed, and purified full-length FleR ($FleR_{FL}$; residues 1–473), REC domain ($FleR_{REC}$, residues 1–129), and N-terminus-deleted ($FleR_{AAA+DBD}$, residues 129–473) FleR constructs (Figure 1A). We assessed the ATPase activity of $FleR_{FL}$ in phosphorylated and non-phosphorylated state. Phosphorylation of the protein was carried out chemically using small molecule phosphodonor, acetyl phosphate (AcP). $FleR_{FL}$ shows low ATPase activity, which increases about 12-fold upon phosphorylation (Figure 1B). Low ATPase activity has also been detected for NtrC4 and NtrC in the non-phosphorylated form.[11,31] In order to rule out partial phosphorylation of $FleR_{FL}$ during purification, which could result in low ATPase activity, phosphorylation was abrogated by substitution of D53 with alanine, and the ATPase activity of the purified protein was measured. The $FleR_{D53A}$ showed similar activity as the $FleR_{FL}$ in non-phosphorylated state. Interestingly, the ATPase activity of the REC-domain-deleted construct ($FleR_{AAA+DBD}$) was 3.3-fold higher compared with non-phosphorylated $FleR_{FL}$; however, it was lower than the activated form of $FleR_{FL}$ (Figure 1B). Overall, we observed that the non-phosphorylated $FleR_{FL}$ is competent for ATP hydrolysis, and this activity is enhanced upon phosphorylation.

Crystal structure of REC domain reveals an active dimer

We determined the crystal structure of $FleR_{REC}$. Phases were obtained by molecular replacement using receiver domain of DctD (PDB: 1QKK) as the search model. Two molecules of $FleR_{REC}$ were present in the asymmetric unit. Data collection and refinement statistics are summarized in Table 1. Each molecule of $FleR_{REC}$ is composed of five parallel β-strands that form the core of the molecule surrounded by five helices forming a typical REC domain fold (Figure 1C). The REC domains of σ^{54} activators are known to exhibit different dimerization interface in the active phosphorylated and inactive non-phosphorylated forms.[32,33] There were four kinds of dimers present in the crystal lattice—AB, AC, AD, and AE with buried surface area (BSA) of 439 $Å^2$, 323 $Å^2$, 510 $Å^2$, and 261 $Å^2$, respectively (Figure 1C). The dimer AD exhibited the major interface formed through contacts between the α4 and β5 of each monomer, which resembled the activated forms of REC domain earlier observed for DctD (PDB:1L5Y) and NtrC1 (PDB:1ZY2). $FleR_{REC}$ AD dimer shows excellent superimposition, with the chain of both DctD and NtrC1 yielding root-mean-square deviation (RMSD) of 1.5 Å and 1.03 Å, respectively (Figure 1D).[32,33]

The aspartate (D53) that undergoes phosphorylation in the motif (EDDK) is present at the end of the β3 and is located in a crevice formed by loop 1, 5, and 7. The crystals of $FleR_{REC}$ were obtained in the presence of calcium acetate; consequently, the structure contains a Ca^{2+} ion coordinated at the active site in place of Mg^{2+} in other structures. D53 interacts with the Ca^{2+} ion and also forms a salt bridge with K103. E9 also forms a salt bridge with K103. The two aspartate residues and one glutamate form a negatively charged acidic pocket. In the current structure, along with D53, D10, and main chain N55, three water molecules stabilize the binding of Ca^{2+} ion, which shows pentagonal-bipyramidal geometry (Figure 1E). Fo-Fc map of the active site is shown in Figure S2. Further, the bond distances between the protein atoms and the ion are within 2.2–2.5 Å, which is characteristic of Ca^{2+} ion.

Superimposition of the current crystal structure on the inactive (non-phosphorylated) form of REC domain observed earlier for NtrC1 (PDB:1NY5) yielded RMSD of 1.3 Å for monomer (Figure 1F).[10] Comparison of the two structures reveals that the structural change occurs in the loop between β4 and α4 upon activation (Figure 1G). The loop partially covers the active site, thus adopting a closed conformation. In case of inactive state observed in NtrC1, the loop points away from the active site (Figure 1G). The activation also involves movement of Tyr83 (His81 in NtrC1) that rotates inward towards the active site and concomitant flipping of Tyr100 (Phe98 in NtrC1). Similarly, the highly conserved Thr81 (Thr79 in NtrC1) moves toward the catalytic center. This reorientation of the key residues Tyr/Phe and Ser/Thr also called as "switch residues" gives rise to twist in β4, which results in displacement of α4. Movement of α4 results in altered dimer interface and lower BSA in the active form. These rearrangements are also consistent with activated structures of DctD.[33] In the current structure, the active

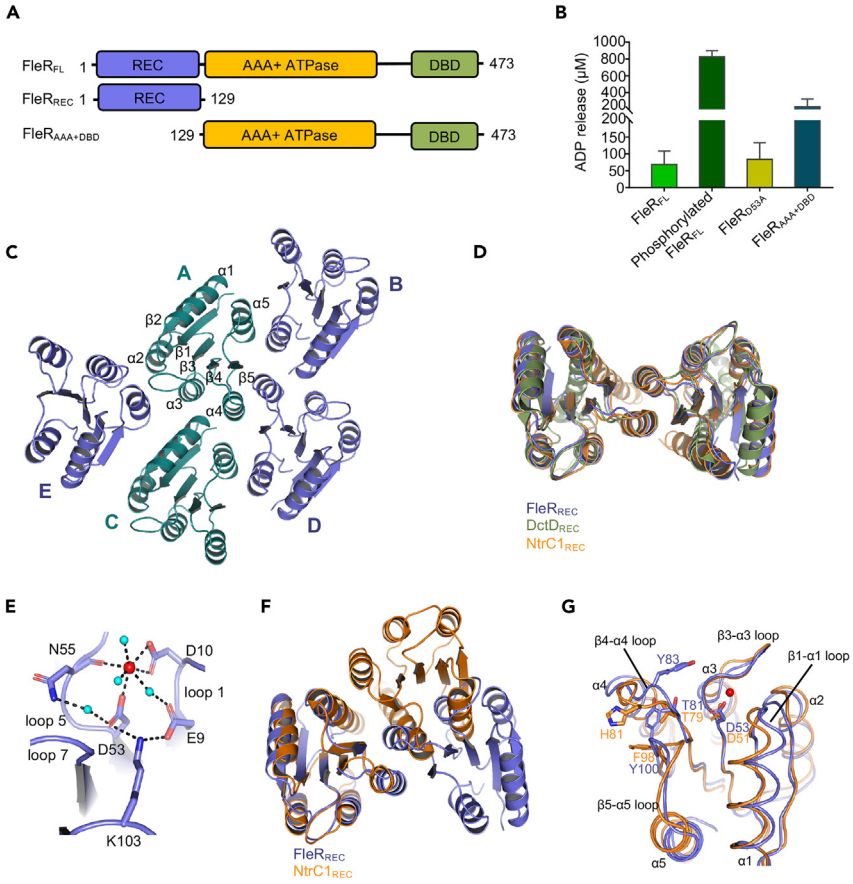

Figure 1. Structure of REC domain

(A) Schematic representation of the FleR constructs used in the manuscript. The domains REC, AAA+, and DBD are shown in purple, yellow, and green, respectively.

(B) The ATPase activity of FleR$_{FL}$ in phosphorylated and non-phosphorylated forms, FleR$_{D53A}$ and FleR$_{AAA+DBD}$, was assayed with 1mM ATP. Amount of ADP released by the protein in 20 min was measured. The error bars were obtained from two independent experiments, each performed in triplicate.

(C) Ribbon representation of FleR$_{REC}$ showing packing in crystal lattice. The monomers are labeled as A, B, C, D, and E. The secondary structural elements are labeled for monomer A.

(D) The active state AD dimer of FleR$_{REC}$ (slate) is superposed on the active state dimer of DctD (PDB:1L5Y, green) and NtrC1 (PDB:1ZY2, orange).

(E) Coordination of calcium ion in the active site of FleR$_{REC}$ is shown. Calcium ion and water molecules are depicted as red and cyan spheres, respectively. Polar interactions that are within 3 Å distance are illustrated as black dashed lines.

(F) Superimposition of active state dimer of FleR$_{REC}$ (AD) on the inactive state dimer of NtrC1 (PDB:1NY5).

(G) Superposition of inactive NtrC1$_{REC}$ (PDB: 1NY5, orange) on active state FleR$_{REC}$ (slate). Side chains of Tyr83, Tyr100, and Thr81 and corresponding side chain in NtrC1, that undergo conformational changes are shown as stick. Protein backbone is shown as tube, and Ca^{2+} ion is depicted as red sphere.

conformation has been achieved in the absence of phosphorylation possibly due to high concentration of protein used for crystallization. Phosphorylation-independent activation has also been observed earlier for RR02rec, ComE$_{REC}$, and Rcp1.[34–36]

Phosphorylation of FleR$_{FL}$ results in oligomer formation

Chemical phosphorylation using AcP followed by dynamic light scattering (DLS) was used to assess the changes in the quaternary structure of FleR$_{FL}$ in solution. DLS shows an increase in the hydrodynamic diameter (12–23 nm) of the protein in phosphorylated state, indicating a change in its oligomeric form (Figure 2A; Table 2). However, FleR$_{D53A}$ showed no change in the diameter, indicating that FleR$_{FL}$ undergoes phosphorylation-dependent oligomer formation (Figures 2B; Table 2). The phosphorylation of the protein was verified using SDS-PAGE containing Phos-Tag, a tag that is included in the gel to separate phosphorylated and non-phosphorylated proteins. The phosphorylated protein shows upward shift, and densitometry indicated phosphorylation of about 80% of FleR$_{FL}$ and no shift in case of FleR$_{D53A}$ mutant (Figure S3).

Next, we used analytical gel filtration to assess the oligomer formation post-phosphorylation in case of the full-length protein. Phosphorylation using AcP resulted in two peaks in SEC, one of which coincides with non-phosphorylated protein, indicating unstable oligomer (Figure 2C). Thus, in order to obtain stable oligomeric protein, we designed a mutant based on the NtrC where replacement of S160 (Ser150 in

Table 1. Data collection and refinement statistics

	$FleR_{REC}$
Data collection	
Space group	$P2_1$
Cell (Å)	33.7, 67.7, 51.4 90.0, 92.2, 90.0
Resolution (Å)[a]	67.71–2.28 (2.35–2.28)
Total no. of reflections	67,359
Unique reflections	10,642
R_{sym} or R_{merg}	0.166 (0.801)
R_{meas}	0.181 (0.878)
R_{pim}	0.072 (0.353)
$I/\delta I$	7.3 (2.2)
Completeness (%)	100 (100)
Correlation $CC_{(1/2)}$	0.983 (0.84)
Multiplicity	6.3 (6)
Refinement	
Resolution (Å)	2.28
R_{work}/R_{free}[b]	18.64/22.10
Average B factors (Å^2)	
Protein: A	33.91
Protein: B	34.14
Ca^{2+}: C	45.2
Acetate: D	58.55
Water: S	39.1
RMSD	
Bond lengths (Å)	0.008
Bond angles (°)	1.005

RMSD, root-mean-square deviation.
[a]The highest-resolution shell is shown in parentheses.
[b]*Rfree* was calculated using 5% of the data excluded from refinement.

case of FleR) with Phe in AAA+ domain led to stabilization of the oligomeric assembly.[8] The purified, phosphorylated form of $FleR_{S150F}$ showed complete shift toward higher molecular weight in analytical gel filtration, whereas the non-phosphorylated $FleR_{S150F}$ shows a broad peak that lies in between phosphorylated and non-phosphorylated states. This suggests that non-phosphorylated $FleR_{S150F}$ mutant forms a mixture of oligomers. We also evaluated the ATPase activity of $FleR_{S150F}$ and found it to be similar to $FleR_{FL}$ upon phosphorylation (Figure 2D). This implies that substitution of S150F results in stabilization of the oligomeric state of $FleR_{FL}$ without affecting its ATPase activity. $FleR_{S150F}$ was thus used for all further analysis.

SAXS of $FleR_{D53A}$, $FleR_{S150F}$, and $FleR_{REC}$

To gain structural insights into the oligomeric assembly of $FleR_{FL}$ in solution in the non-phosphorylated state and the conformational changes linked to activation post phosphorylation, we collected solution SAXS data for the non-phosphorylated $FleR_{D53A,}$ phosphorylated form of $FleR_{S150F}$, and non-phosphorylated $FleR_{REC}$. Monodispersity was ensured before and after phosphorylation prior to SAXS experiment (Table 2).

Figure 3A shows experimental SAXS curves for three different concentration series for all three protein samples. SAXS data obtained from lowest dilution series were used for further analysis. The Guinier and normalized Kratky plots for all the three states of the protein are shown in Figures S4A and S4B, respectively, which confirm that proteins are well folded. Further, normalized pair distance distribution functions (P(r)) for all three samples were calculated, and the plot shows the dimensions of the protein samples in solution (Figure S4C). The bead models were generated using DAMMIF. These were further clustered using DAMCLUST of ATSAS suite (Table S1).[37] The cluster with maximum number of models represents the envelop generated by DAMAVER. The envelop generated using DAMFILT was used for model fitting. Table 3

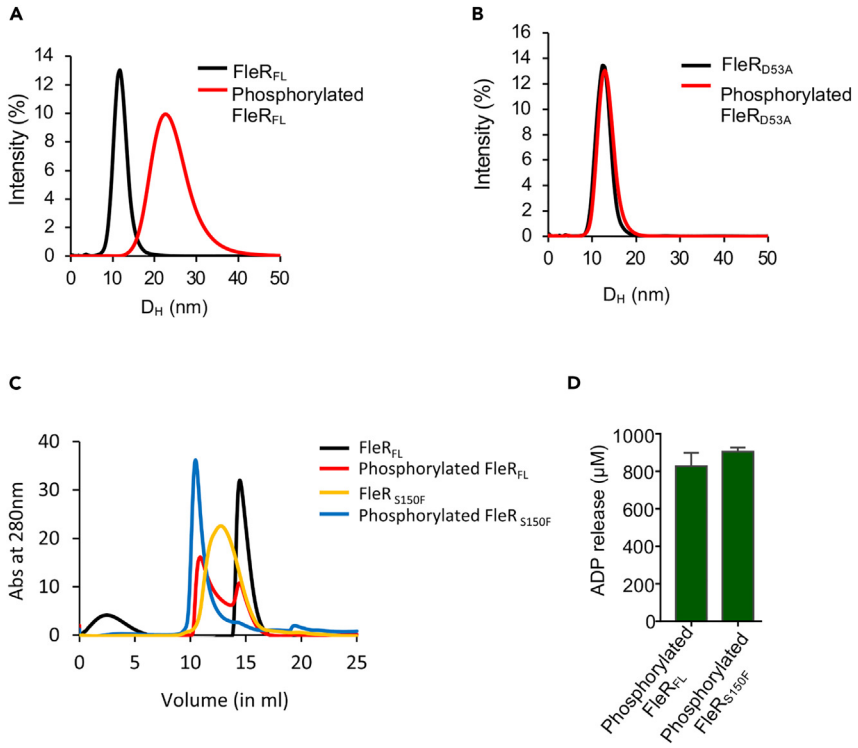

Figure 2. Size distribution of phosphorylated and non-phosphorylated FleR

(A and B) Hydrodynamic diameters of FleR$_{FL}$ and FleR$_{D53A}$ are shown in non-phosphorylated (black line) and phosphorylated states (red line).

(C) Superdex 200 10/300 size-exclusion chromatogram showing the elution volume of phosphorylated FleR$_{FL}$ (red line), non-phosphorylated FleR$_{FL}$ (black line), non-phosphorylated FleR$_{S150F}$ (golden line), and phosphorylated FleR$_{S150F}$ (blue line).

(D) The ATPase activity of FleR$_{FL}$ and FleR$_{S150F}$ in phosphorylated states was assayed with 1mM ATP. Amount of ADP released by the proteins in 20 min was measured. The error bars represent standard deviations from two independent experiments, each performed in triplicate.

summarizes the size parameters including the protein molecular weight, the maximum dimensions of the particle (D_{max}), and radius of gyration (R_g), which provides an estimate of the overall particle size.

The SAXS-derived molecular weight of FleR$_{D53A}$ in the non-phosphorylated form was ~113 kDa, which corresponds well with the theoretical molecular weight of ~103 kDa for a dimer. The structures of NtrC1 (REC-AAA+), NtrC4 (REC-AAA+), and NtrX (Full length) have been captured as dimers in the inactive state.[10,11,38] Although NtrC1 and NtrX dimers are stabilized by the long coiled-coiled linkers between the REC and AAA+ domains, the structure of NtrC4 (REC-AAA+) on the other hand has unstructured linker between REC and AAA+ domains and hence forms a weaker dimer. The dimeric contacts in all these proteins are present in all the three domains. Compared with these proteins, the linker in FleR is very short (14 amino acids). To discern the dimeric interface, we performed chemical crosslinking of FleR$_{REC}$, FleR$_{DBD}$, and FleR$_{AAA+}$ in the inactive state. The crosslinking gels show that although the FleR$_{DBD}$ forms dimers in solution, the FleR$_{REC}$ domain was monomeric and FleR$_{AAA+}$ formed various oligomeric assemblies (Figure S5).

To fit the model in the envelope, we first generated the AlphaFold2 models of individual domains, which were then used for modeling the dimer of FleR$_{AAA+}$ and FleR$_{DBD}$ based on the quaternary structure of NtrC4, which shows 41% identity with FleR (highest among the available dimeric structures; PDB: 3DZD and 4FTH).[11,39] The predicted local distance difference test (pLDDT) score for AlphaFold2 model was higher than 70 for FleR$_{REC}$, FleR$_{AAA+}$, and FleR$_{DBD}$ and was below 50 for the linker regions (Figure S6). Two independent monomers of REC domains and the dimer of FleR$_{AAA+}$ and FleR$_{DBD}$ were docked into the SAXS envelop as shown in Figure 3B with the χ^2 of 2.28.

Molecular weight for non-phosphorylated REC domain estimated by SAXS (14.8 kDa) correlated well with molecular mass for a monomer (14.3 kDa). A monomer of the FleR$_{REC}$ was docked into the envelop of REC domain yielding χ^2 of 3.6 (Figure 3C). The average structure of non-phosphorylated FleR$_{D53A}$ and FleR$_{REC}$ is depicted in Figures 3B and 3C. Figure S7 shows scattering intensity of models overlapped with the experimental data, which indicated a good fit.

SAXS of FleR$_{S150F}$ reveals formation of heptamers upon phosphorylation

We next aimed to assess the nature of conformational changes in FleR$_{S150F}$ on phosphorylation, using SAXS. The Bayesian calculations of molecular mass for phosphorylated FleR$_{S150F}$ (~318 kDa) corresponds to the molecular weight of a heptamer (360.5 kDa being the theoretical molecular mass). This also correlates with the higher hydrodynamic diameter of FleR$_{FL}$ observed in DLS and analytical gel filtration (Figures 2A and 2C).

Table 2. Hydrodynamic diameter of $FleR_{FL}$ and $FleR_{D53A}$

	D_H(nm) in non-phosphorylated state	Polydispersity index (PDI) in non-phosphorylated state	D_H(nm) in phosphorylated state	Polydispersity index (PDI) in phosphorylated state
$FleR_{FL}$	12.14 ± 0.65	0.146 ± 0.01	23.17 ± 0.58	0.077 ± 0.02
$FleR_{D53A}$	12.33 ± 0.97	0.170 ± 0.05	12.7 ± 0.33	0.171 ± 0.01

The heptameric ring of FleR was generated on the basis of quaternary structure of FlrC AAA+ domain (63% identity for the AAA+ domain of FlrC with FleR, PDB: 4QHS) by superimposition of seven monomeric $FleR_{AAA+}$ domains.[13] The AAA+ domain was first placed in the central portion of the density. We next placed the high-resolution crystal structure of activated REC domain in the remaining volume of the density such that it is packed against the AAA+ domain in a way to facilitate the interaction between the amino acids present in the α4 of REC and α1 of the AAA+ domain (Figure 4A). It may be noted that the α4 of REC undergoes a conformational change upon activation as seen in the crystal structure mentioned earlier (Figures 1E and 1F). This helix is buried in the inactive state of REC domain. Activation exposes α4 that forms the dimer interface in crystals of REC domain alone. However, we postulated that in the presence of AAA+ domain, this α4 interface will participate in heptamer formation and will interact with the α/β subdomain of ATPase domain (Figure 4B). The interface is lined by Arg residues (R138, R146) in the AAA+ domain that may form salt bridges with the negatively charged residues of REC domain. Location of REC is also consistent with the biochemical data on NtrC, predicting interaction between α4 of REC and α1 of the AAA+ domain in the activated state.[40,41]

The linker between AAA+ and DBD for $FleR_{FL}$ is proline rich and unusually long (~53 residues) compared with other EBPs that contain DBD (Figure S1). It is hence likely to be unstructured and flexible. The DNA-binding domains hence could not be located in the SAXS envelop. The DNA-binding domains typically are located at the bottom of the ring. However, there was no space in the SAXS envelop to accommodate these domains (Figure 4A). It has been seen that the position of the DBD with respect to the AAA+ ring alters during the ATP hydrolysis cycle.[8] During the transition state, when the EBP contacts the σ^{54} through the GAFTGA loop, the DNA-binding domains are packed closer to the central ring. After hydrolysis, and disengagement of the GAFTGA loop, the DNA-binding domains lose association with the central ring. Because no nucleotide was added for SAXS experiment in FleR, and in the absence of any protrusion from the central core, it appears that the structure of the oligomeric form of $FleR_{S150F}$ captured in this study is in post hydrolytic state. Overall, placement of the model of $FleR_{AAA+}$ and crystal structure of $FleR_{REC}$ domains within the SAXS envelop showed good correspondence and reasonable fit. The final χ^2 obtained for the $FleR_{S150F}$ was 12.4 in P7 symmetry (Figure 4A).

α1 of $FleR_{AAA+}$ interacts with α4 of $FleR_{REC}$

In order to validate the assignment of $FleR_{REC}$ location in the activated form, we substituted R146, which is present on $FleR_{AAA+}$ and plausibly interacts with D87 on REC domain to glutamic acid. Full-length purified $FleR_{R146E}$ was subjected to analytical size exclusion chromatography in the phosphorylated and non-phosphorylated form. It was found that in both the forms, $FleR_{R146E}$ elutes at the same volume that coincides with the non-phosphorylated $FleR_{FL}$, indicating disruption of the oligomeric state (Figure S8A).

We also performed *in vivo* complementation assays with $FleR_{R146E}$. We complemented the *fleR* knockout mPAO1 strain of *Pseudomonas aeruginosa* with the $fleR_{R146E}$, integrated on a plasmid pHERD20T, and examined the motility of the strain on soft agar plate by recording the diameter of the motility zone (Figure 4C). The wild-type (wt) strain exhibited diameter of 2.6 cm (Figure 4D), but knock out of *fleR* was defective in motility. Complementation of the full-length *fleR* restores motility to the wild-type levels. However, the $fleR_{R146E}$ remained at the point of inoculation and yielded a diameter of 0.6 cm, suggesting impaired motility (Figures 4C and 4D). This validates the placement of REC domain in the active state.

Additionally, we also complemented the knock out with $fleR_{S150F}$ variant that was used for SAXS in the active state. It shows motility equivalent to $fleR_{FL}$ (Figures 4C and 4D). However, complementation with $fleR_{AAA+DBD(S150F)}$ does not restore the motility of the bacteria, which suggests S150F substitution is not adequate and REC domain is essential for stabilization of the active form of the protein (Figures 4C and 4D).

We also investigated the effect of substitution of $fleR_{R146E}$ and $fleR_{S150F}$ on flagellar phenotype, using transmission electron microscopy. mPAO1 strain harbors a single polar flagellum, whereas Δ*fleR* strain was aflagellate (Figures 4E and 4F). Complementation of the knockout strain with full-length *fleR* restores the wild-type phenotype. Strikingly, the strain complemented with $fleR_{R146E}$ shows defect in flagella formation; however, $fleR_{S150F}$ showed single polar flagella (Figures 4E and 4F). Thus, perturbation of the observed interface between REC and AAA+ domain leads to motility and flagella formation defects, validating the interface between REC and AAA+ domain.[40]

Negative staining microscopy of $FleR_{S150F}$

To investigate if there are large-scale conformational/oligomeric changes in the protein during ATP hydrolysis, dynamic light scattering of phosphorylated $FleR_{S150F}$ was carried out in the presence of ADP (adenosine-di-phosphate), ADP-AlF_3 (transition state mimic), and non-hydrolysable analog, ATPγS (Adenosine 5′-[γ-thio]triphosphate). ATPγS is frequently used to trap the ground state of the protein, whereas the ADP-AlF_3 is used to trap the transition state during ATP hydrolysis. ADP would represent the product bound form of the protein. The result shows that the hydrodynamic diameter of the protein remains same in the presence of all the three nucleotides (Figure 5A). Additionally, in analytical size exclusion chromatography phosphorylated $FleR_{S150F}$ elutes at the same volume in ADP- and ADP-AlF_3-bound states (Figure S8B).

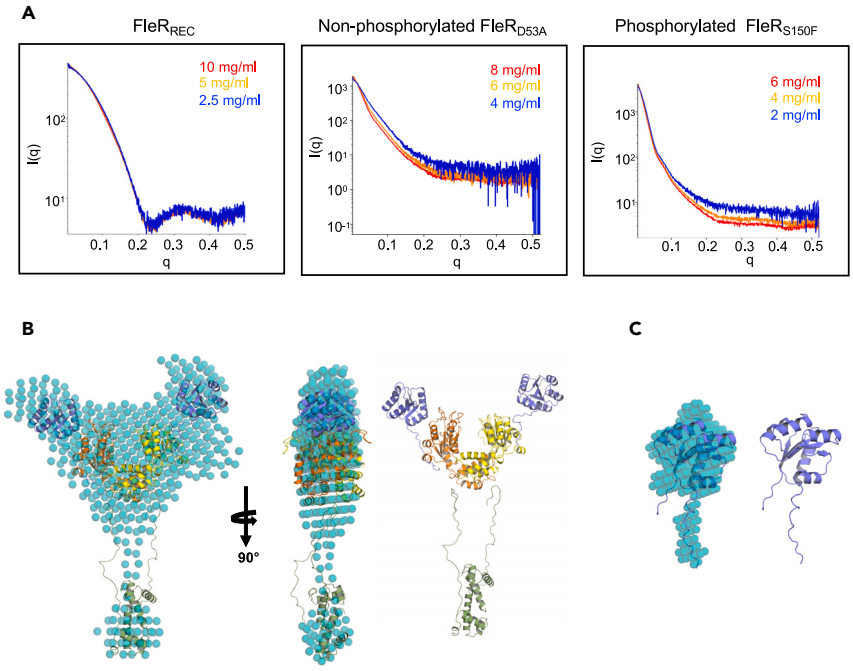

Figure 3. Solution conformation of FleR

(A) Superimposition of experimental scattering plot of FleR$_{REC}$, inactive FleR$_{D53A}$, and active FleR$_{S150F}$ at three different concentrations are shown. (B and C) The ribbon representation of FleR$_{D53A}$ and FleR$_{REC}$ fitted within the respective SAXS envelops (shown as cyan beads) in non-phosphorylated states. The REC domain is depicted in slate; FleR$_{AAA+}$ is in orange and yellow, and FleR$_{DBD}$ is in green.

We next sought to visualize the oligomeric assembly using negative staining transmission electron microscopy. Purified FleR$_{S150F}$ was subjected to AcP in the presence of saturating conditions of Mg^{+2} and ADP. The protein was then applied to carbon-coated grids and negatively stained with uranyl acetate followed by analysis using electron microscopy. We acquired 205 micrographs and picked 40,676 particles using cryoSPARC v.4.1.[42] 2D classification was performed, and good class averages were selected (17,656 particles). 2D class averages revealed that particles had ring-like appearance with 7-fold symmetry (Figures 5B and 5C). Each distinct ring has a diameter of about ~165 Å. Representative raw electron micrograph and the 2D class averages are shown in Figures 5B and 5C. Small blobs of globular density were observed (marked with arrows) extending outward from the donut-shaped rings in some particles (Figure 5C). Three thousand seven hundred fifty-seven particles were used for reconstruction of ab initio map. Clear density for one and weak density for the second blob, representing the NTD, was evident surrounding the central core (Figure 5D). Further, 7-fold symmetry (C7) was applied, and map was generated (Figure 5E). The SAXS structure of the heptamer of FleR$_{S150F}$ was docked manually using UCSF Chimera into the 3D envelop generated using negative staining EM density map (Figure 5F).[43] When fitted into the map, the model produced correlation coefficient of 0.63 with the NTD overlapping with the extra density visible outside of the central ring. It was observed that the density for the NTD, although present, was weaker than the central ring, which could be attributed to interaction being transient. Again, the density for DNA-binding domain could not be located.

Deletion of REC domain results in motility defects and aflagellate phenotype in *P. aeruginosa*

From the aforementioned structural analysis, it appeared that the REC domain stabilizes the AAA+ domain of FleR. In order to further assess the role of REC domain in stabilization of the oligomeric assembly, we performed dynamic light scattering with the FleR$_{AAA+DBD}$ construct, which shows that the hydrodynamic diameter of FleR$_{AAA+DBD}$ is higher than non-phosphorylated FleR$_{FL}$ but lower than the phosphorylated FleR$_{FL}$, indicating potential failure to form the functional oligomeric form (Figure 6A). We next estimated the motility of complemented *fleR*$_{AAA+DBD}$ in *fleR* knockout strain of *P. aeruginosa* on soft agar plates. Interestingly, complementation of Δ*fleR*$_{FL}$ strain with the plasmid containing *fleR*$_{AAA+DBD}$ exhibited smaller diameter similar to Δ*fleR*$_{FL}$, indicating defective motility. *fleR*$_{D53A}$ complementation also showed similar phenotype (Figures 6B and 6C). These results establish that the presence of REC domain of FleR$_{FL}$ is essential for flagellar-based motility. Additionally, TEM images of the Δ*fleR* strain complemented with *fleR*$_{AAA+DBD}$ or *fleR*$_{D53A}$ shows defect in flagella formation and yielded aflagellate phenotype, confirming that the REC domain of FleR and its phosphorylation are vital for flagellar assembly (Figures 6D and 6E).

FleR$_{FL}$ directly activates the transcription of *flgB* and *flgF* genes that code for basal body rod formation in *Pseudomonas aeruginosa*. Next, we performed real-time quantitative PCR experiment to assess the effect of deletion of REC domain on transcription regulation by FleR$_{FL}$. As expected, Δ*fleR*$_{FL}$ exhibits low level of expression for both the genes, whereas the expression was restored upon complementation of the full length *fleR*. However, *fleR*$_{AAA+DBD}$- or *fleR*$_{D53A}$-complemented bacterial strains show reduced expression of *flgB and flgF* genes compared

Table 3. Small-angle X-ray scattering (SAXS) data collection and statistics

	$FleR_{REC}$	Non-phosphorylated $FleR_{D53A}$	Phosphorylated $FleR_{S150F}$
Data collection parameters			
X-ray source	BM29, ESRF	BM29, ESRF	BM29, ESRF
Detector	Pilatus 1D	Pilatus 1D	Pilatus 1D
Wavelength (Å)	0.99186	0.99186	0.99186
Exposure time per frame	1 s	1 s	1 s
No. of frames collected	10	10	10
Concentration (mg/mL)	2.5	4	2
Measurement temperature (ºC)	10	10	10
Structural parameters			
I(0) [from Guinier]	113.84	318.4	1061
Rg (nm) [from Guinier]	1.92	5.5	7.46
I(0) [from *P(r)*]	113.5	318.4	1061
R_g (nm) [from *P(r)*]	1.93	5.54	7.5
Porod volume ($Å^3$)	28477.20	185179	1094460
D_{max} (nm)	6.42	20.6	27.19
SAXS derived Molecular Mass			
SAXS MW from Bayesian inference (Da)	14825	113650	318450
Molecular mass from sequence (Da)	14264	103110	360885
Modeling parameters			
Symmetry	P1	P1	P7
Chi^2[a]	1.0	1.2	1.2
Ab initio analysis	DAMMIF	DAMMIF	DAMMIF
NSD	1.28 ± 0.112	1.15 ± 0.16	0.95 ± 0.09

NSD, normalized standard deviation.
[a]Value derived from DAMMIF model.

with mPAO1 or strain complemented with $fleR_{FL}$ (Figure 6F). Thus, these data confirm that REC domain is essential for stability of the oligomeric assembly and transcription initiation.

DISCUSSION

The bEBPs that contain REC domain follow two distinct mechanisms for signal transduction to the catalytic AAA+ domain and consequently have been categorized as positively and negatively regulated response regulators. Typically, these proteins contain two linker regions, one between the REC and AAA+ domain and the other between the AAA+ and the DNA-binding domain (Figure S1). The sequence and length of the linker regions is correlated with the kind of regulatory mechanism followed by the bEBP.[11,32] The negative regulators such as NtrC1 and DctD are dimers in the inactive state, and the ATPase activity is curbed by the REC domain in this non-phosphorylated state.[10,33] This is possible owing to the front-to-front dimers stabilized by structured coiled-coil linker between the REC and AAA+ domain that forms a part of dimer interface. Thus, long linker is suggestive of negative regulation. This arrangement is incompatible with oligomer formation. Presence of "GHG" motif in REC domain has been predicted to be another indicator of strong dimer of regulatory domain and hence is associated with negative regulatory mechanism. Phosphorylation of the third aspartate in the D(E)DDK motif present in the REC domain releases this repression and enables the formation of front to back dimers, an arrangement that coincides with oligomerization. Deletion of the REC domain of the negatively regulated proteins thus favors the formation of the constitutive active oligomers.[32]

The structural and biochemical data in the current study permit us to categorize FleR as bEBP that follows a positive regulatory mechanism. Unlike in the case of negative regulators, the linker between the REC and AAA+ domains is short and unstructured as evident from SAXS and multiple sequence alignment (Figure S1). It is unlikely to form coiled-coil in the non-phosphorylated state, resulting in weak interactions between the monomers in the inactive form. This flexibility of linker is also responsible for inadequate repression of ATPase activity in dimeric form. Thus, an increase in protein concentration might also be enough to push the equilibrium toward the oligomeric state. The absence of "GHG" motif further endorses positive regulatory mechanism in FleR (Figure S1). We also demonstrate that deletion of REC domain destabilizes oligomer and results in non-functional protein *in vivo*. This implies that, once activated, the REC domain of one protomer must contact

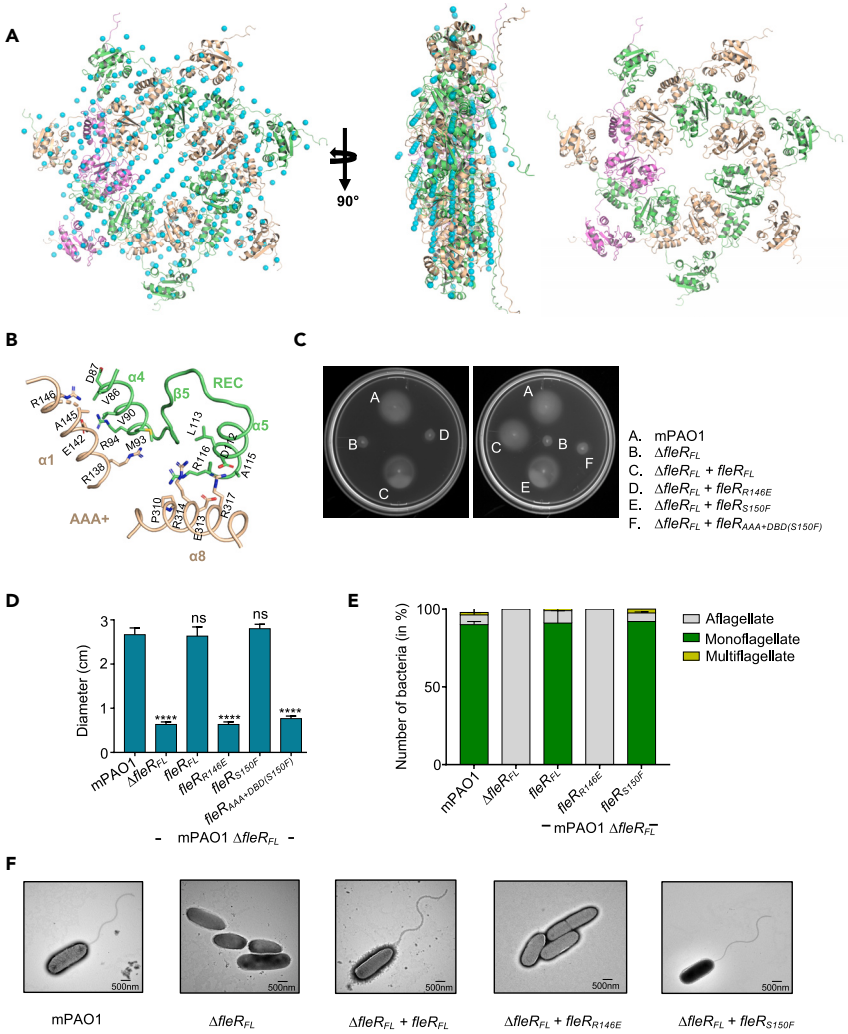

Figure 4. Solution conformation of phosphorylated FleR

(A) Fitting of the model of $FleR_{S150F}$ (with P7 symmetry) encompassing AAA+ and REC domains (protomers colored alternatively wheat, lime green, and pink as an odd protomer) within the SAXS-derived envelop of phosphorylated $FleR_{S150F}$. Two views related by 90° are shown.

(B) Interactions of REC domain (lime green) with the AAA+ domain (wheat) in the activated state are depicted for one set of protomer. The side chains that were within the 3.5 Å distance between the two domains have been displayed as stick.

(C) Swimming motility of wild-type *P. aeruginosa* (mPAO1), $fleR_{FL}$ knockout ($\Delta fleR_{FL}$), and $fleR_{FL}$ knockout strain complemented with either full-length *fleR* ($\Delta fleR_{FL}$ + $fleR_{FL}$), $fleR_{R146E}$ ($\Delta fleR_{FL}$ + $fleR_{R146E}$), $fleR_{S150F}$ ($\Delta fleR_{FL}$ + $fleR_{S150F}$), or $fleR_{AAA+DBD(S150F)}$ ($\Delta fleR_{FL}$ + $fleR_{AAA+DBD(S150F)}$) is shown.

(D) The bar graph shows comparison of swimming zones. Error bars represent the standard deviations, N = 3. The statistical significance (p value) was calculated by unpaired Student's t test (****$p \leq 0.0001$; $^{ns}p > 0.05$) by keeping mPAO1 as a control.

(E) Statistical analysis of flagellar phenotype of different strains of *Pseudomonas aeruginosa* wild-type, knockout ($\Delta fleR_{FL}$) and knockout strain complemented with wild-type *fleR* or its variants is shown. Gray, green, and yellow bars denote aflagellate, monoflagellate, and multiflagellate phenotypes, respectively. Error bars represent the standard deviation where N=3.

(F) Transmission electron micrograph showing the flagella phenotype in wild-type *P. aeruginosa* (mPAO1), $\Delta fleR_{FL}$, and $\Delta fleR_{FL}$ complemented with $fleR_{FL}$, $fleR_{R146E}$, and $fleR_{S150F}$. The scale bar is 500 nm.

the AAA+ domain of the adjacent protomer, stabilizing the heptameric assembly. This mode of inter-subunit interaction has also been seen for NtrC, another regulator that follows a positive regulatory mechanism.[8] NtrC4 on the other hand follows a hybrid mechanism where the buried surface area between the REC domain in inactive state is less compared with NtrC1, and REC is not required to facilitate the assembly of the active form.[11]

The oligomeric stoichiometry of NtrC family members has been investigated extensively. Although hexameric form of EBP is more favourable, both hexameric and heptameric ensembles have been observed. While AAA+ domain of NtrC1 and FlrC forms heptamers, PspF and AAA+DBD domain of ZraR form hexameric rings.[9,10,12,13] Interestingly, full-length activated NtrC4 and the one lacking the DNA-binding

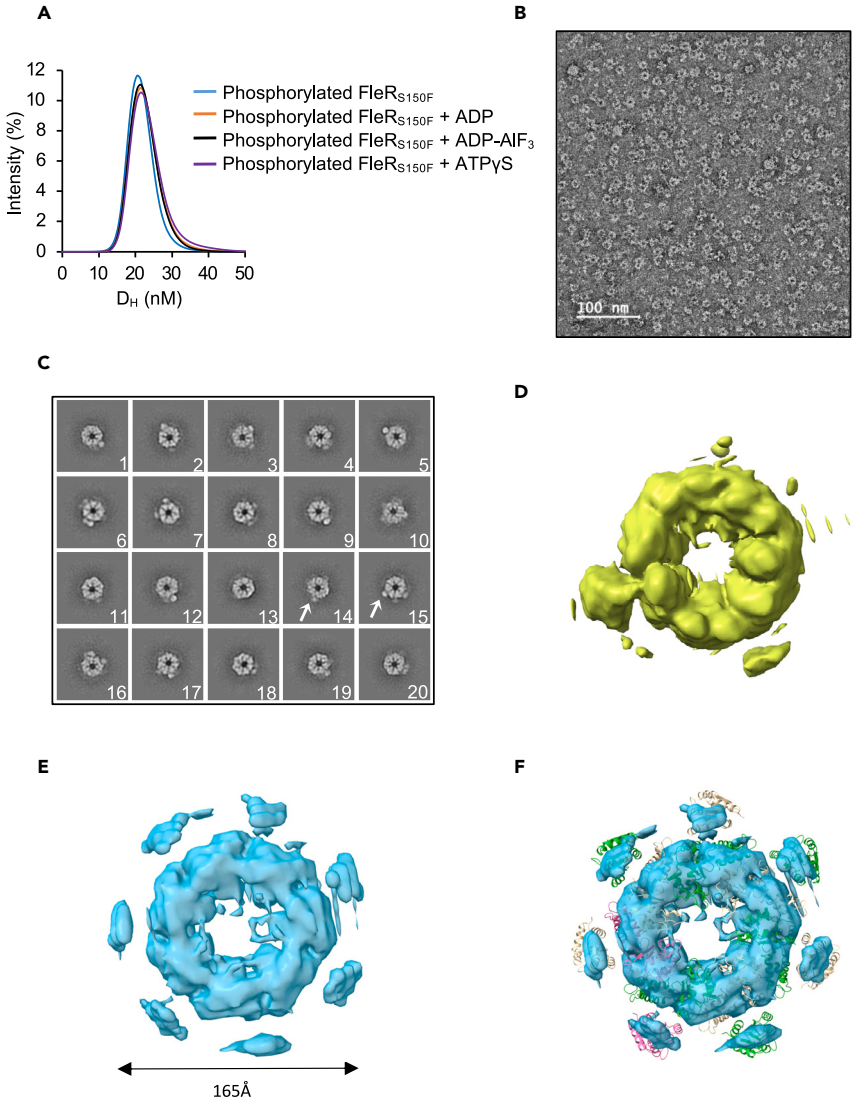

Figure 5. Structure of $FleR_{S150F}$ by negative staining

(A) Hydrodynamic diameter of phosphorylated $FleR_{S150F}$ alone (blue line), with ADP (orange line), ADP-AlF_3 (black line), and ATPγS (violet line).

(B) Negative stain image of phosphorylated $FleR_{S150F}$.

(C) 2D class averages of $FleR_{S150F}$ show a heptameric arrangement.

(D) Ab initio 3D map of phosphorylated $FleR_{S150F}$.

(E) 3D map with C7 symmetry generated from 2D class average showing heptameric assembly of the protein, with arrow showing the diameter of the model.

(F) The fit of the SAXS model of $FleR_{S150F}$ on to the 3D EM model.

domain form hexamers ,whereas isolated AAA+ domain and AAA+ domain with DNA-binding domain form heptamers.[44] Some AAA+ ATPases have been shown to switch between the two stoichiometric arrangements.[45] Such versatility in assembly can be caused by the presence or absence of substrate and/or the nucleotide. Presence of different stoichiometric arrangements also reveals the plasticity of the AAA+ domains and offers insights into the intermediate states during the process of assembly or function. We observed that $FleR_{S150F}$ forms heptamers in presence of ADP. We also observed that deletion of REC domain results in non-functional protein *in vivo*. The deletion of the REC domain possibly leads to destabilization of the heptamer and formation of smaller oligomeric forms of the protein. This could result in slight increase in ATPase activity as observed here. Thus, REC domain through its interaction with adjacent AAA+ domain stabilizes the formation of the oligomeric assembly. However, other stoichiometric arrangements for FleR cannot be ruled out in presence of non-hydrolyzable ATP or during transition state.

Structural and biochemical studies have also pointed toward the structural asymmetry in the ring architecture of bEBPs due to interconversion between ATP binding and release.[45,46] It has been proposed that the conformational differences between the subunits are essential for interaction of bEBPs with σ^{54}-RNAP. Formation of the oligomer creates the central pore, and the two conserved loops L1 and L2 face the

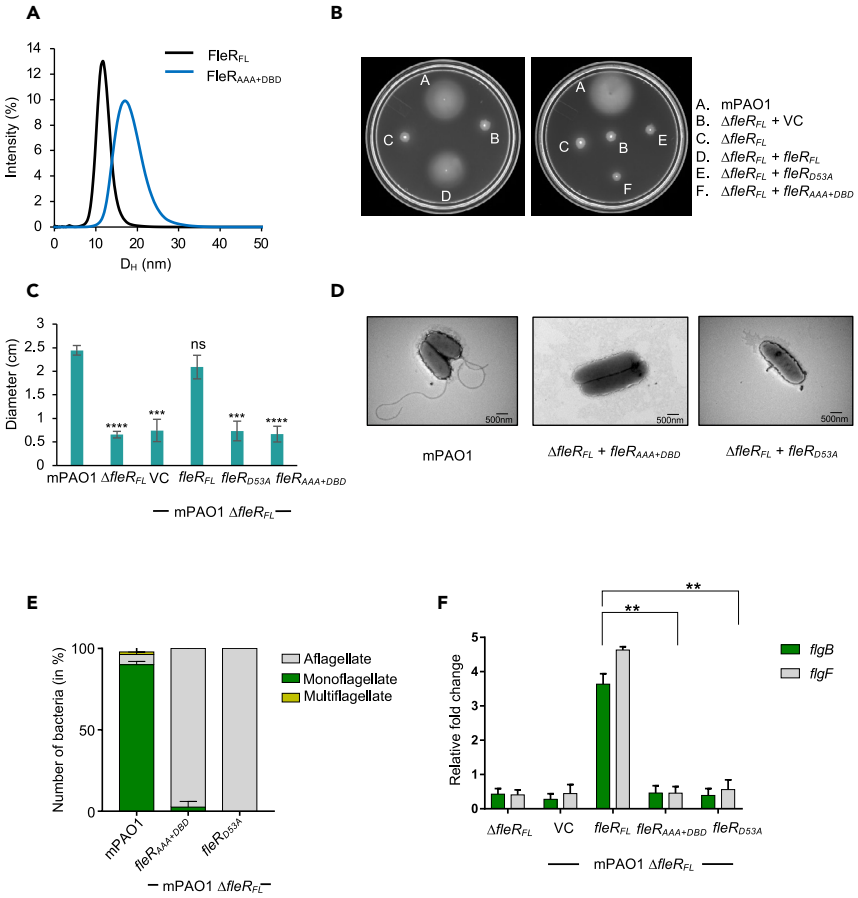

Figure 6. Role of REC in stabilization of oligomer

(A) The hydrodynamic diameters of non-phosphorylated FleR (black line) and $FleR_{AAA+DBD}$ (blue line) are shown.

(B) Swimming motility of wild-type *P. aeruginosa* (mPAO1), *fleR*$_{FL}$ knockout (Δ*fleR*$_{FL}$), and *fleR*$_{FL}$ knockout strain complemented with either full-length *fleR* (*ΔfleR*$_{FL}$ + *fleR*$_{FL}$) or *fleR*$_{D53A}$ mutant (Δ*fleR*$_{FL}$ + *fleR*$_{D53A}$) or REC deleted *fleR* (*ΔfleR*$_{FL}$ + *fleR*$_{AAA+DBD}$) or the empty vector (*ΔfleR*$_{FL}$ + *VC*).

(C) The bar graph shows comparison of swimming zones. Error bars represent the standard deviations, N = 3. The statistical significance (p value) was calculated by unpaired Student's t test (***p ≤ 0.001; ****p ≤ 0.0001; ^{ns}p > 0.05) using mPAO1 as a control.

(D) Transmission electron micrograph showing the flagellar phenotype in wild-type *P. aeruginosa* (mPAO1) and Δ*fleR*$_{FL}$ complemented with *fleR*$_{AAA+DBD}$. The scale bar is 500 nm.

(E) Statistical analysis of flagellar phenotype of strains complemented with mutant *fleR* of *Pseudomonas aeruginosa* is shown. Gray, green, and yellow bars denote aflagellate, monoflagellate, and multiflagellate phenotypes, respectively. Error bars represent the standard deviation where N=3.

(F) Relative *flgB* and *flgF* transcript levels were checked in wild-type *P. aeruginosa* (mPAO1), Δ*fleR*$_{FL}$, and complemented Δ*fleR*$_{FL}$ with various constructs. The *rpoD* (σ^{70}) was used as the reference gene for fold-change calculation. Error bars represent the standard deviations, N = 2. The statistical significance (p value) was calculated by unpaired Student's t test (**p ≤ 0.01).

lumen of the pore. The L1 loop harbors the conserved signature sequence GAFTGA. ATP hydrolysis by bEBPs reorganizes σ^{54} such that the inhibition imposed by its N-terminus on formation of open complex is removed. Recent CryoEM structure of the transition state complex of PspF-σ^{54}-RNAP-promoter reveals that the activator forms a non-planar hexameric ring with L1 loops forming a spiral, which engage with N-terminus of σ^{54} facilitating open complex formation.[7,12] The pseudo symmetry of the oligomeric form guided by nucleotide binding drives the conformational switching of the L1 pore loop that remodels the σ^{54}-RNAP complex.[7,12,45] However, AAA+ domain of FlrC, the functional homolog of FleR in *Vibrio*, forms symmetric heptamers where all protomers bind ATP simultaneously for concerted hydrolysis.[13]

FleR forms one of the regulatory checkpoints in the flagellar assembly that controls the expression of hook and rod genes post-assembly of flagellar export apparatus. The complexity involving several regulatory checkpoints in the transcriptional circuitry is advantageous for assembly of the composite machinery such as the flagellum with high precision and efficiency. Further, it makes the assembly responsive to a variety of environmental and cellular cues. Our data reveal that FleR follows a positive regulatory mechanism where the non-phosphorylated form is a weak dimer and has low ATPase activity. This may be essential for expression of flagellar gene at the level required for its maintenance. Complete revocation of ATPase activity in the non-phosphorylated state would result in complete shutdown of the flagellar cascade. Thus, positive

regulators allow for fine-tuning the transcription rather than operate like an on-off switch. Negative regulators on the other hand may be essential for functions that require stringent environmental signals for activation.

Limitations of the study

We have assessed the oligomeric state of full-length FleR in phosphorylated and non-phosphorylated states. The results reveal that the protein forms heptameric arrangement facilitated by the REC domain upon phosphorylation. The overall hypothesis of our study is validated by both *in vivo* and *in vitro* assays. However, high-resolution structural data are required to obtain atomic level details of the interactions between REC and AAA+ domain, as well as to determine the position of the DNA-binding domain in the heptamer.

STAR★METHODS

Detailed methods are provided in the online version of this paper and include the following:

- KEY RESOURCES TABLE
- RESOURCE AVAILABILITY
  - Lead contact
  - Materials availability
  - Data and code availability
- EXPERIMENTAL MODEL AND STUDY PARTICIPANT DETAILS
  - Bacterial strains
- METHOD DETAILS
  - Cloning of FleR and its constructs
  - Protein expression and purification
  - ATPase assay
  - Crystallization, data collection and refinement of $FleR_{REC}$
  - *In vitro* phosphorylation and phos-tag gel electrophoresis
  - Analytical size exclusion chromatography
  - Small angle X-ray scattering (SAXS)
  - Dynamic light scattering (DLS)
  - Negative staining of protein and visualization in TEM
  - Transmission electron microscopy of bacteria
  - In-solution chemical cross-linking
  - Motility assay
  - RNA extraction and quantitative real-time PCR (qRT PCR)
- QUANTIFICATION AND STATISTICAL ANALYSIS

SUPPLEMENTAL INFORMATION

Supplemental information can be found online at https://doi.org/10.1016/j.isci.2023.108397.

ACKNOWLEDGMENTS

We acknowledge the help rendered by Dr. Petra Pernot and Dr. Dihia Moussaoui (BM29 beamline, ESRF) for SAXS data collection and Prof. Deepak T. Nair for X-ray data collection at the X06DA beamline of Swiss Light Source (SLS), Switzerland. We acknowledge Prof. D.N. Rao for providing plasmid pHERD20T for complementation assays. We thank Priya Srivastava for help with cloning. We also thank Reena Rani and Madhava Rao M for help with the TEM experiments that were carried out at ATPC-RCB. The work was supported by intramural funds available from the Regional Centre for Biotechnology to D.J. R.C.B. is funded by Department of Biotechnology, Ministry of Science and Technology, Government of India. P.K.S. is supported by the fellowship from Council of Scientific and Industrial Research. Sheenu is supported by fellowship from University Grants Commission. D.J. acknowledges ESRF Access Program of RCB (supported by the grant number BT/PR36150/INF/22/214/2020 of the Department of Biotechnology, Ministry of Science and Technology). Manoil lab prepared *Pseudomonas aeruginosa* mutant library using the National Institute of Health grant # NIH P30 DK089507.

AUTHOR CONTRIBUTIONS

P.K.S. cloned; purified protein; performed biochemical experiments, model building, and refinement; analyzed structural data; and prepared figures. S. performed *in vivo* experiments. D.J. conceptualized, acquired funding, supervised research, performed structural analysis, and wrote the manuscript.

DECLARATION OF INTERESTS

The authors declare no competing interests.

INCLUSION AND DIVERSITY

We support inclusive, diverse, and equitable conduct of research.

Received: April 22, 2023
Revised: September 12, 2023
Accepted: November 2, 2023
Published: November 4, 2023

REFERENCES

1. Ishimoto, K.S., and Lory, S. (1989). Formation of pilin in Pseudomonas aeruginosa requires the alternative σ factor (RpoN) of RNA polymerase. Proc. Natl. Acad. Sci. USA *86*, 1954–1957. https://doi.org/10.1073/pnas.86.6.1954.
2. Shao, X., Zhang, X., Zhang, Y., Zhu, M., Yang, P., Yuan, J., Xie, Y., Zhou, T., Wang, W., Chen, S., et al. (2018). RpoN-dependent direct regulation of quorum sensing and the type VI secretion system in Pseudomonas aeruginosa PAO1. J. Bacteriol. *200*, e00205-18. https://doi.org/10.1128/JB.00205-18.
3. Ferro-Luzzi Ames, G., and Nikaido, K. (1985). Nitrogen regulation in Salmonella typhimurium. Identification of an ntrC protein-binding site and definition of a consensus binding sequence. EMBO J. *4*, 539–547. https://doi.org/10.1002/j.1460-2075.1985.tb03662.x.
4. Flores-Kim, J., and Darwin, A.J. (2016). The Phage Shock Protein Response. Annu. Rev. Microbiol. *70*, 83–101. https://doi.org/10.1146/ANNUREV-MICRO-102215-095359.
5. Chanchal, Banerjee, P., Raghav, S., Goswami, H.N., and Jain, D. (2021). The antiactivator FleN uses an allosteric mechanism to regulate σ54-dependent expression of flagellar genes in Pseudomonas aeruginosa. Sci. Adv. *7*, eabj1792. https://doi.org/10.1126/SCIADV.ABJ1792.
6. Bush, M., and Dixon, R. (2012). The Role of Bacterial Enhancer Binding Proteins as Specialized Activators of σ 54 -Dependent Transcription. Microbiol. Mol. Biol. Rev. *76*, 497–529. https://doi.org/10.1128/mmbr.00006-12.
7. Ye, F., Gao, F., Liu, X., Buck, M., and Zhang, X. (2022). Mechanisms of DNA opening revealed in AAA+ transcription complex structures. Sci. Adv. *8*, eadd3479. https://doi.org/10.1126/SCIADV.ADD3479.
8. De Carlo, S., Chen, B., Hoover, T.R., Kondrashkina, E., Nogales, E., and Nixon, B.T. (2006). The structural basis for regulated assembly and function of the transcriptional activator NtrC. Genes Dev. *20*, 1485–1495. https://doi.org/10.1101/gad.1418306.
9. Sallai, L., and Tucker, P.A. (2005). Crystal structure of the central and C-terminal domain of the σ54-activator ZraR. J. Struct. Biol. *151*, 160–170. https://doi.org/10.1016/j.jsb.2005.05.006.
10. Lee, S.Y., De La Torre, A., Yan, D., Kustu, S., Nixon, B.T., and Wemmer, D.E. (2003). Regulation of the transcriptional activator NtrC1: Structural studies of the regulatory and AAA+ ATPase domains. Genes Dev. *17*, 2552–2563. https://doi.org/10.1101/gad.1125603.
11. Batchelor, J.D., Doucleff, M., Lee, C.J., Matsubara, K., De Carlo, S., Heideker, J., Lamers, M.H., Pelton, J.G., and Wemmer, D.E. (2008). Structure and Regulatory Mechanism of Aquifex aeolicus NtrC4: Variability and Evolution in Bacterial Transcriptional Regulation. J. Mol. Biol. *384*, 1058–1075.
12. Glyde, R., Ye, F., Darbari, V.C., Zhang, N., Buck, M., and Zhang, X. (2017). Structures of RNA Polymerase Closed and Intermediate Complexes Reveal Mechanisms of DNA Opening and Transcription Initiation. Mol. Cell *67*, 106–116.e4. https://doi.org/10.1016/J.MOLCEL.2017.05.010.
13. Dey, S., Biswas, M., Sen, U., and Dasgupta, J. (2015). Unique ATPase Site Architecture Triggers cis-Mediated Synchronized ATP Binding in Heptameric AAA+-ATPase Domain of Flagellar Regulatory Protein FlrC. J. Biol. Chem. *290*, 8734–8747. https://doi.org/10.1074/JBC.M114.611434.
14. Ritchings, B.W., Almira, E.C., Lory, S., and Ramphal, R. (1995). Cloning and phenotypic characterization of fleS and fleR, new response regulators of Pseudomonas aeruginosa which regulate motility and adhesion to mucin. Infect. Immun. *63*, 4868–4876. https://doi.org/10.1128/iai.63.12.4868-4876.1995.
15. Mascher, T., Helmann, J.D., and Unden, G. (2006). Stimulus Perception in Bacterial Signal-Transducing Histidine Kinases. Microbiol. Mol. Biol. Rev. *70*, 910–938. https://doi.org/10.1128/MMBR.00020-06.
16. Terashima, H., Kojima, S., and Homma, M. (2008). Chapter 2 Flagellar Motility in Bacteria: Structure and Function of Flagellar Motor. Int. Rev. Cell Mol. Biol. *270*, 39–85. https://doi.org/10.1016/S1937-6448(08)01402-0.
17. Dasgupta, N., Wolfgang, M.C., Goodman, A.L., Arora, S.K., Jyot, J., Lory, S., and Ramphal, R. (2003). A four-tiered transcriptional regulatory circuit controls flagellar biogenesis in Pseudomonas aeruginosa. Mol. Microbiol. *50*, 809–824.
18. Banerjee, P., Chanchal, and Jain, D. (2019). Sensor i Regulated ATPase Activity of FleQ Is Essential for Motility to Biofilm Transition in Pseudomonas aeruginosa. ACS Chem. Biol. *14*, 1515–1527. https://doi.org/10.1021/acschembio.9b00255.
19. Chanchal, Banerjee, P., and Jain, D. (2017). ATP-Induced Structural Remodeling in the Antiactivator FleN Enables Formation of the Functional Dimeric Form. Structure *25*, 243–252. https://doi.org/10.1016/J.STR.2016.11.022.
20. Harshita, Chanchal, and Jain, D. (2016). Cloning, expression, purification, crystallization and initial crystallographic analysis of FleN from Pseudomonas aeruginosa. Acta Crystallogr. F Struct. Biol. Commun. *72*, 135–138. https://doi.org/10.1107/S2053230X16000170.
21. Zhou, T., Huang, J., Liu, Z., Xu, Z., and Zhang, L.H. (2021). Molecular Mechanisms Underlying the Regulation of Biofilm Formation and Swimming Motility by FleS/FleR in Pseudomonas aeruginosa. Front. Microbiol. *12*, 707711.
22. Zhou, T., Huang, J., Feng, Q., Liu, Z., Lin, Q., Xu, Z., and Zhang, L.-H. (2021). A Two-Component System FleS/FleR Regulates Multiple Virulence-Related Traits in Pseudomonas aeruginosa. Preprint at bioRxiv. https://doi.org/10.1101/2021.04.22.441042.
23. Correa, N.E., Lauriano, C.M., McGee, R., and Klose, K.E. (2000). Phosphorylation of the flagellar regulatory protein FlrC is necessary for Vibrio cholerae motility and enhanced colonization. Mol. Microbiol. *35*, 743–755. https://doi.org/10.1046/J.1365-2958.2000.01745.X.
24. Joslin, S.N., and Hendrixson, D.R. (2008). Analysis of the Campylobacter jejuni FlgR response regulator suggests integration of diverse mechanisms to activate an NtrC-like protein. J. Bacteriol. *190*, 2422–2433. https://doi.org/10.1128/JB.01827-07.
25. Shi, M., Gao, T., Ju, L., Yao, Y., and Gao, H. (2014). Effects of FlrBC on flagellar biosynthesis of Shewanella oneidensis. Mol. Microbiol. *93*, 1269–1283. https://doi.org/10.1111/MMI.12731.
26. Burnham, P.M., Kolar, W.P., and Hendrixson, D.R. (2020). A polar flagellar transcriptional program mediated by diverse two-component signal transduction systems and basal flagellar proteins is broadly conserved in polar flagellates. mBio *11*, e03107-19. https://doi.org/10.1128/MBIO.03107-19.
27. Niehus, E., Gressmann, H., Ye, F., Schlapbach, R., Dehio, M., Dehio, C., Stack, A., Meyer, T.F., Suerbaum, S., and Josenhans, C. (2004). Genome-wide analysis of transcriptional hierarchy and feedback regulation in the flagellar system of Helicobacter pylori. Mol. Microbiol. *52*, 947–961.
28. Gellatly, S.L., Bains, M., Breidenstein, E.B.M., Strehmel, J., Reffuveille, F., Taylor, P.K., Yeung, A.T.Y., Overhage, J., and Hancock, R.E.W. (2018). Novel roles for two-component regulatory systems in cytotoxicity and virulence-related properties in Pseudomonas aeruginosa. AIMS Microbiol. *4*, 173–191. https://doi.org/10.3934/microbiol.2018.1.173.
29. Joly, N., Zhang, N., and Buck, M. (2012). ATPase Site Architecture Is Required for Self-Assembly and Remodeling Activity of a Hexameric AAA+ Transcriptional Activator. Mol. Cell *47*, 484–490. https://doi.org/10.1016/J.MOLCEL.2012.06.012.
30. Chen, B., Sysoeva, T.A., Chowdhury, S., Guo, L., De Carlo, S., Hanson, J.A., Yang, H., and Nixon, B.T. (2010). Engagement of Arginine Finger to ATP Triggers Large Conformational Changes in NtrC1 AAA+ ATPase for Remodeling Bacterial RNA Polymerase. Structure *18*, 1420–1430. https://doi.org/10.1016/J.STR.2010.08.018.

31. Weiss, D.S., Batut, J., Klose, K.E., Keener, J., and Kustu, S. (1991). The phosphorylated form of the enhancer-binding protein NTRC has an ATPase activity that is essential for activation of transcription. Cell *67*, 155–167. https://doi.org/10.1016/0092-8674(91)90579-N.
32. Doucleff, M., Chen, B., Maris, A.E., Wemmer, D.E., Kondrashkina, E., and Nixon, B.T. (2005). Negative regulation of AAA+ ATPase assembly by two component receiver domains: A transcription activation mechanism that is conserved in mesophilic and extremely hyperthermophilic bacteria. J. Mol. Biol. *353*, 242–255. https://doi.org/10.1016/j.jmb.2005.08.003.
33. Park, S., Meyer, M., Jones, A.D., Yennawar, H.P., Yennawar, N.H., and Nixon, B.T. (2002). Two-component signaling in the AAA + ATPase DctD: binding Mg2+ and BeF3-selects between alternate dimeric states of the receiver domain. FASEB J *16*, 1964–1966. https://doi.org/10.1096/FJ.02-0395FJE.
34. Bent, C.J., Isaacs, N.W., Mitchell, T.J., and Riboldi-Tunnicliffe, A. (2004). Crystal Structure of the Response Regulator 02 Receiver Domain, the Essential YycF Two-Component System of Streptococcus pneumoniae in both Complexed and Native States. J. Bacteriol. *186*, 2872–2879. https://doi.org/10.1128/JB.186.9.2872-2879.2004.
35. Im, Y.J., Rho, S.-H., Park, C.-M., Yang, S.-S., Kang, J.-G., Lee, J.Y., Song, P.-S., and Eom, S.H. (2002). Crystal structure of a cyanobacterial phytochrome response regulator. Protein Sci. *11*, 614–624. https://doi.org/10.1110/ps.39102.
36. Boudes, M., Sanchez, D., Graille, M., Van Tilbeurgh, H., Durand, D., and Quevillon-Cheruel, S. (2014). Structural insights into the dimerization of the response regulator ComE from Streptococcus pneumoniae. Nucleic Acids Res. *42*, 5302–5313. https://doi.org/10.1093/NAR/GKU110.
37. Petoukhov, M.V., Franke, D., Shkumatov, A.V., Tria, G., Kikhney, A.G., Gajda, M., Gorba, C., Mertens, H.D.T., Konarev, P.V., and Svergun, D.I. (2012). New developments in the ATSAS program package for small-angle scattering data analysis. J. Appl. Crystallogr. *45*, 342–350. https://doi.org/10.1107/S0021889812007662.
38. Fernández, I., Cornaciu, I., Carrica, M.D.C., Uchikawa, E., Hoffmann, G., Sieira, R., Márquez, J.A., Márquez, J.A., and Goldbaum, F.A. (2017). Three-Dimensional Structure of Full-Length NtrX, an Unusual Member of the NtrC Family of Response Regulators. J. Mol. Biol. *429*, 1192–1212. https://doi.org/10.1016/j.jmb.2016.12.022.
39. Vidangos, N.K., Heideker, J., Lyubimov, A., Lamers, M., Huo, Y., Pelton, J.G., Ton, J., Gralla, J., Berger, J., and Wemmer, D.E. (2014). DNA-recognition by a σ54 transcriptional activator from Aquifex aeolicus. J. Mol. Biol. *426*, 3553–3568. https://doi.org/10.1016/J.JMB.2014.08.009.
40. Lee, J., Owens, J.T., Hwang, I., Meares, C., and Kustu, S. (2000). Phosphorylation-induced signal propagation in the response regulator NtrC. J. Bacteriol. *182*, 5188–5195. https://doi.org/10.1128/JB.182.18.5188-5195.2000.
41. Hastings, C.A., Lee, S.Y., Cho, H.S., Yan, D., Kustu, S., and Wemmer, D.E. (2003). High-resolution solution structure of the beryllofluoride-activated NtrC receiver domain. Biochemistry *42*, 9081–9090. https://doi.org/10.1021/bi0273866.
42. Punjani, A., Rubinstein, J.L., Fleet, D.J., and Brubaker, M.A. (2017). cryoSPARC: algorithms for rapid unsupervised cryo-EM structure determination. Nat. Methods *143*, 290–296. https://doi.org/10.1038/nmeth.4169.
43. Pettersen, E.F., Goddard, T.D., Huang, C.C., Couch, G.S., Greenblatt, D.M., Meng, E.C., and Ferrin, T.E. (2004). UCSF Chimera - A visualization system for exploratory research and analysis. J. Comput. Chem. *25*, 1605–1612. https://doi.org/10.1002/jcc.20084.
44. Batchelor, J.D., Sterling, H.J., Hong, E., Williams, E.R., and Wemmer, D.E. (2009). Receiver domains control the active state stoichiometry of Aquifex aeolicus σ54 activator NtrC4, as revealed by electrospray mass spectrometry. J. Mol. Biol. *393*, 634–643. https://doi.org/10.1016/J.JMB.2009.08.033.
45. Sysoeva, T.A., Chowdhury, S., Guo, L., Nixon, B.T., and Nixon, B.T. (2013). Nucleotide-induced asymmetry within ATPase activator ring drives σ54–RNAP interaction and ATP hydrolysis. Genes Dev. *27*, 2500–2511. https://doi.org/10.1101/GAD.229385.113.
46. Schumacher, J., Joly, N., Claeys-Bouuaert, I.L., Aziz, S.A., Rappas, M., Zhang, X., and Buck, M. (2008). Mechanism of homotropic control to coordinate hydrolysis in a hexameric AAA+ ring ATPase. J. Mol. Biol. *381*, 1–12. https://doi.org/10.1016/J.JMB.2008.05.075.
47. Evans, P.R., and Murshudov, G.N. (2013). How good are my data and what is the resolution? Acta Crystallogr. D Biol. Crystallogr. *69*, 1204–1214. https://doi.org/10.1107/S0907444913000061.
48. Winter, G., Waterman, D.G., Parkhurst, J.M., Brewster, A.S., Gildea, R.J., Gerstel, M., Fuentes-Montero, L., Vollmar, M., Michels-Clark, T., Young, I.D., et al. (2018). DIALS: implementation and evaluation of a new integration package. Acta Crystallogr. D Struct. Biol. *74*, 85–97. https://doi.org/10.1107/S2059798317017235.
49. McCoy, A.J., Grosse-Kunstleve, R.W., Adams, P.D., Winn, M.D., Storoni, L.C., and Read, R.J. (2007). Phaser crystallographic software. J. Appl. Crystallogr. *40*, 658–674. https://doi.org/10.1107/S0021889807021206.
50. Emsley, P., Lohkamp, B., Scott, W.G., and Cowtan, K. (2010). Features and development of Coot. Acta Crystallogr. D Biol. Crystallogr. *66*, 486–501. https://doi.org/10.1107/S0907444910007493.
51. Adams, P.D., Afonine, P.V., Bunkóczi, G., Chen, V.B., Davis, I.W., Echols, N., Headd, J.J., Hung, L.W., Kapral, G.J., Grosse-Kunstleve, R.W., et al. (2010). PHENIX: a comprehensive Python-based system for macromolecular structure solution. Acta Crystallogr. D Biol. Crystallogr. *66*, 213–221. https://doi.org/10.1107/S0907444909052925.
52. Winn, M.D., Isupov, M.N., and Murshudov, G.N. (2001). Use of TLS parameters to model anisotropic displacements in macromolecular refinement. Acta Crystallogr. D Biol. Crystallogr. *57*, 122–133. https://doi.org/10.1107/S0907444900014736.
53. Manalastas- Cantos, K., Konarev, P. V., Hajizadeh, N. R., Kikhney, A. G., Petoukhov, M. V., Molodenskiy, D. S., Panjkovich, A., Mertens, H.D.T., Gruzinov, A., Borges, C.M., Svergun, D.I., and Franke, D. (2021). ATSAS 3.0: expanded functionality and new tools for small-angle scattering data analysis. J. Appl. Crystallogr. *54*, 343–355. https://doi.org/10.1107/S1600576720013412.
54. Hopkins, J.B., Gillilan, R.E., and Skou, S. (2017). BioXTAS RAW: improvements to a free open-source program for small-angle X-ray scattering data reduction and analysis. J. Appl. Crystallogr. *50*, 1545–1553. https://doi.org/10.1107/S1600576717011438.
55. Franke, D., and Svergun, D.I. (2009). DAMMIF, a program for rapid ab-initio shape determination in small-angle scattering. J. Appl. Crystallogr. *42*, 342–346. https://doi.org/10.1107/S0021889809000338.
56. Yang, J., Anishchenko, I., Park, H., Peng, Z., Ovchinnikov, S., and Baker, D. (2020). Improved protein structure prediction using predicted interresidue orientations. Proc. Natl. Acad. Sci. USA *117*, 1496–1503. https://doi.org/10.1073/pnas.1914677117.
57. Svergun, D., Barberato, C., and Koch, M.H.J. (1995). CRYSOL – a Program to Evaluate X-ray Solution Scattering of Biological Macromolecules from Atomic Coordinates. J. Appl. Crystallogr. *28*, 768–773. https://doi.org/10.1107/S0021889895007047.
58. Franke, D., Petoukhov, M.V., Konarev, P.V., Panjkovich, A., Tuukkanen, A., Mertens, H.D.T., Kikhney, A.G., Hajizadeh, N.R., Franklin, J.M., Jeffries, C.M., and Svergun, D.I. (2017). ATSAS 2.8: A comprehensive data analysis suite for small-angle scattering from macromolecular solutions. J. Appl. Crystallogr. *50*, 1212–1225. https://doi.org/10.1107/S1600576717007786.
59. Panjkovich, A., and Svergun, D.I. (2016). Deciphering conformational transitions of proteins by small angle X-ray scattering and normal mode analysis. Phys. Chem. Chem. Phys. *18*, 5707–5719. https://doi.org/10.1039/C5CP04540A.

STAR★METHODS

KEY RESOURCES TABLE

REAGENT or RESOURCE	SOURCE	IDENTIFIER
Bacterial and virus strains		
Pseudomonas aeruginosa (mPAO1)	Manoil lab, UAS	https://www.gs.washington.edu/labs/manoil/libraryindex.htm
Pseudomonas aeruginosa (*ΔfleR*)	Manoil lab, UAS	https://www.gs.washington.edu/labs/manoil/libraryindex.htm
Chemicals, peptides, and recombinant proteins		
Acetyl phosphate	Sigma	Cat#A0262
Tris	GoldBio	Cat#T-400-500
PEG 5K MME	Sigma	Cat#81323
Sulfo-EGS	Sigma	Cat# 803219
Coomassie Brillant Blue G-250	Sigma	Cat# 1.15444
Trizol	Invitrogen	Cat# 15596026
Critical commercial assays		
QuikChange II XL Site-Directed Mutagenesis Kit	Agilent	Cat# 210519
ADP-Glo kinase assay kit	Promega	Cat#V6930
SuperScript III Platinum SYBR Green One-Step qRT-PCR Kit	Invitrogen	Cat#11736059
RNeasy® Mini kit	Qiagen	Cat# 74004
Deposited data		
$FleR_{REC}$ domain structure	This Paper	PDB: 7W9H
Oligonucleotides		
5′-ACATACCATATGATGGCAGCCAAAGTCCTGCTGGTC	This Paper	$FleR_{FL}$ –F
5′-ACATACGGATCCTCAGATGGCGTAGAGATAGGCCTC	This Paper	$FleR_{FL}$ –R
5′-ACATACCATATGGGTCCGGTGGCCCTGGAGC	This Paper	$FleR_{AAA+,DBD}$ -F
5′-ACATACGGATCCTCAGATGGCGTAGAGATAGGCCTC	This Paper	$FleR_{AAA+,DBD}$ -R
5′-ACATACCATATGGGTCCGGTGGCCCTGGAGC	This Paper	$FleR_{AAA+}$ -F
5′-ACATACGGATCCTCACGCGGTGAGGCACAGGTCG	This Paper	$FleR_{AAA+}$ -R
5′-GGAGGATGGTTAGGTGGCCCT	This Paper	$FleR_{REC}$ -F
5′-AGGGCCACCTAACCATCCTCC	This Paper	$FleR_{REC}$ -R
5′-ACATACGGTACCATGGCAGCCAAAGTCCTGCTGGTC	This Paper	$FleR_{FL}$ –F_pHERD20T
5′-ACATACAAGCTTTCAGATGGCGTAGAGATAGGCCTC	This Paper	$FleR_{FL}$ -R_pHERD20T
5′-ACATACGGTACCGGTCCGGTGGCCCTGGAGC	This Paper	$FleR_{AAA+,DBD}$ -F_pHERD20T
5′-ACATACAAGCTTTCAGATGGCGTAGAGATAGGCCTC	This Paper	$FleR_{AAA+,DBD}$ -R_pHERD20T
5′-GGTGATCAGCGCCGTGAACATGC	This Paper	$FleR_{D53A}$ -F
5′-GCATGTTCACGGCGCTGATCACC	This Paper	$FleR_{D53A}$ -R
5′-ACTGGCCGCGGAGGTCGCGCGC	This Paper	$FleR_{R146E}$ -F
5′-GCGCGCGACCTCCGCGGCCAGT	This Paper	$FleR_{R146E}$ -R
5′-CGGGTCGCGCGCTTCGATTCCACCGTG	This Paper	$FleR_{S150F}$ -F
5′-CACGGTGGAATCGAAGCGCGCGACCCG	This Paper	$FleR_{S150F}$ -R
Recombinant DNA		
Plasmid: modified pET14b-6xHis-SUMO-tag-PreScission Protease site-NdeI-*fleR*$_{FL}$-BamHI	This Paper	

(*Continued on next page*)

Continued

REAGENT or RESOURCE	SOURCE	IDENTIFIER
Plasmid: modified pET14b-6xHis-SUMO-tag-PreScission Protease site-NdeI-*fleR*$_{REC}$-BamHI	This Paper	
Plasmid: modified pET14b-6xHis-SUMO-tag-PreScission Protease site-NdeI-*fleR*$_{AAA+}$-BamHI	This Paper	
Plasmid: modified pET14b-6xHis-SUMO-tag-PreScission Protease site-NdeI-*fleR*$_{AAA+DBD}$-BamHI	This Paper	
Plasmid: modified pET14b-6xHis-SUMO-tag-PreScission Protease site-NdeI-*fleR*$_{DBD}$-BamHI	This Paper	
Plasmid: modified pET14b-6xHis-SUMO-tag-PreScission Protease site-NdeI-*fleR*$_{S150F}$-BamHI	This Paper	
Plasmid: modified pET14b-6xHis-SUMO-tag-PreScission Protease site-NdeI-*fleR*$_{D53A}$-BamHI	This Paper	
Plasmid: modified pET14b-6xHis-SUMO-tag-PreScission Protease site-NdeI-*fleR*$_{R146E}$-BamHI	This Paper	
Plasmid: pHERD20T- *fleR*$_{FL}$	This Paper	
Plasmid: pHERD20T- *fleR*$_{D53A}$	This Paper	
Plasmid: pHERD20T- *fleR*$_{R146E}$	This Paper	
Plasmid: pHERD20T- *fleR*$_{AAA+DBD}$	This Paper	
Software and algorithms		
DIALS of CCP4 i2	(Winter et al., 2018)	https://www.ccp4.ac.uk/
AIMLESS of CCP4	(Evans & Murshudov, 2013)	https://www.ccp4.ac.uk/
Structure Refinement: PHENIX	(Adams et al., 2010)	http://www.phenix-online.org/
Structure Modelling: COOT	(Emsley et al., 2010)	https://www.ccp4.ac.uk/
PyMol 2.3	Schrödinger, LLC	https://pymol.org/
PRIMUS (ATSAS 3.0.4 software package)	(Konarev et al., 2003)	https://www.embl-hamburg.de/biosaxs/primus.html
BioXTAS RAW	(Hopkins et al., 2017)	https://bioxtas-raw.readthedocs.io/en/latest/
DAMMIF	(Franke & Svergun, 2009)	https://www.embl-hamburg.de/biosaxs/dammif.html
GASBOR	(Svergun et al., 2001)	https://www.embl-hamburg.de/biosaxs/gasbor.html
SREFLEX	(Panjkovich & Svergun, 2016)	https://www.embl-hamburg.de/biosaxs/sreflex.html
CRYSOL 2.0 and CRYSOL 3.0	(Svergun et al., 1995; Franke et al., 2017)	https://www.embl-hamburg.de/biosaxs/crysol.html
SITUS		https://situs.biomachina.org/
UCSF CHIMERA	(Pettersen et al., 2004)	https://www.cgl.ucsf.edu/chimera/

RESOURCE AVAILABILITY

Lead contact

Further information and requests should be directed to the lead contact, Deepti Jain (deepti@rcb.res.in).

Materials availability

This study did not generate new unique reagents. Plasmids used in this study are available on request after completion of a Materials Transfer Agreement.

Data and code availability

- Data reported in this paper will be shared by the lead contact upon request.
- Atomic coordinates and structure factors have been deposited in the PDB with accession code 7W9H.
- This paper does not report original code.
- Any additional information required to reanalyze the data reported in this paper is available from the lead contact upon request.

EXPERIMENTAL MODEL AND STUDY PARTICIPANT DETAILS

Bacterial strains

This work used *P. aeruginosa* (mPAO1) for *in vivo* experiments. The proteins were recombinantly expressed in *Escherichia coli* B834 (DE3). The details of the growth conditions are mentioned in STAR Methods section.

METHOD DETAILS

Cloning of FleR and its constructs

The FleR gene (*Pseudomonas* genome DB: PA1099) was cloned into a modified pET14b vector containing N-terminus His_6-SUMO tag. $FleR_{FL}$ was PCR amplified from genomic DNA of *P. aeruginosa* (PAO1 strain) using gene specific primer containing *Nde*I and *Bam*HI restriction site. Cloning of $FleR_{AAA+DBD}$ (129-473 residues), $FleR_{AAA+}$ (129-375) and $FleR_{DBD}$ (412-473) was carried out using plasmid containing full length FleR as the template. $FleR_{REC}$ domain construct was made by introducing a stop codon after 129th amino acid residue in full length gene. $FleR_{FL}$ and $FleR_{AAA+DBD}$ were also cloned into pHERD20T vector in *Kpn*I and *Hind*III restriction sites. The D53A, S150F and R146E substitutions were prepared in the respective plasmids using QuikChange II XL site-directed mutagenesis kit (Agilent Technologies). The cloned genes and mutants were confirmed by sequencing at the Advanced Technology Platform Centre (ATPC), RCB.

Protein expression and purification

$FleR_{FL}$, $FleR_{REC}$, $FleR_{AAA+DBD}$, $FleR_{AAA+}$, $FleR_{DBD,}$ $FleR_{D53A}$, $FleR_{S150F}$ and $FleR_{R146E}$ were over expressed in *Escherichia coli* B834 (DE3) cells. Transformed cells were grown in Luria-Bertani media till OD_{600} reach 0.6-0.8 followed by induction using 0.25 mM isopropyl β-d-1-thiogalactopyranoside (IPTG) at 18°C for 16 hrs. Cells were harvested by centrifugation and the respective constructs were resuspended in lysis buffer (25 mM Tris pH 8.0, 500 mM NaCl, 5% glycerol, 5 mM β-mercaptoethanol, and 1 mM PMSF). Cells were lysed by sonication and the lysates were centrifuged at 15,000 rpm for 1 hr. Supernatants were filtered and loaded onto high trap Ni-NTA column (GE Healthcare). The proteins were eluted using a gradient of imidazole. Precision protease was added to the eluted proteins to cleave the His_6-SUMO tag, and dialyzed overnight at 4°C. $FleR_{FL}$, $FleR_{AAA+DBD}$, $FleR_{D53A}$ $FleR_{S150F}$ and $FleR_{R146E}$ were further purified by heparin chromatography before subjecting the protein to size-exclusion chromatography using Superdex 200 16/600 (GE Healthcare) column equilibrated with buffer containing 25 mM Tris pH 8, 250 mM NaCl, 5% glycerol, and 2 mM DTT. $FleR_{AAA+}$ was purified by Ni-NTA affinity chromatography followed by size exclusion using Superdex 200.. Superdex 75 16/600 (GE Healthcare) column was used for $FleR_{REC}$ and $FleR_{DBD}$ after affinity chromatography. The eluted proteins were concentrated and stored in -80°C.

ATPase assay

The ATPase activity of $FleR_{FL}$, $FleR_{AAA+DBD}$, $FleR_{D53A}$ and $FleR_{S150F}$ was measured using the ADP-Glo kinase assay kit (Promega). The reactions were setup in 96 well plate as per the manufacturer's protocol. Phosphorylation of the protein was carried out by incubating the protein with 30 mM acetyl phosphate for 30 min at 4°C. The assay was performed in the buffer containing 50 mM Tris pH 7.5, 10 mM $MgCl_2$ at room temperature (25°C) for 20 minutes using 2.5 μM of protein and 1 mM of ATP. The luminescence signal corresponding to the ADP released was recorded in GloMax 96 microplate luminometer (Promega). A standard curve with luminescent signal as a function of ADP concentration was used to calculate the amount of ADP released during the assay. The graph was plotted in GraphPad Prism 7. All the experiments were performed in triplicates and two independent experiments were used to calculate the standard deviations.

Crystallization, data collection and refinement of $FleR_{REC}$

Crystallization conditions for $FleR_{REC}$ were screened using hanging drop vapour diffusion method using commercially available screens. $FleR_{REC}$ was crystallized in 20% PEG 5K MME and 200 mM calcium acetate. Thin needle like crystals developed after 2 days at 8°C. Crystals were cryoprotected in 40% PEG 5K MME and 200 mM calcium acetate and flash frozen in liquid nitrogen for data collection. X-ray diffraction data were collected at X06DA beamline of Swiss Light Source (SLS), Switzerland. The data were processed with DIALS of CCP4 i2 and scaling was performed in AIMLESS of CCP4 program suite and showed the presence of two molecules in the asymmetric unit.[47,48] The $FleR_{REC}$ structure was determined using molecular replacement (MR) method using the receiver domain structure of DctD (PDB: 1QKK) as the search model.[49] Model building and crystallographic refinement were carried out with Coot (Crystallographic Object-Oriented Toolkit) and the PHENIX program package, respectively.[50,51] During the final round of refinement TLS restraints were applied in PHENIX.[52] PyMol 2.3 (https://pymol.org/) was used to generate the figures.

In vitro phosphorylation and phos-tag gel electrophoresis

10 μM of $FleR_{FL}$ and $FleR_{S150F}$ and $FleR_{D53A}$ was phosphorylated using 30 mM AcP (acetyl phosphate) in buffer containing 25 mM Tris pH 8, 250 mM NaCl, 5% glycerol and 10 mM $MgCl_2$. Phosphorylation was performed at ice for 1 hr and the phosphorylated fraction of protein was separated by Phos-tag (FUJIFILM) SDS-PAGE. The phos-tag SDS-PAGE protocol was adopted from Fernández et al. 2017.[38] Fraction of phosphorylated protein was calculated by ImageJ software.

Analytical size exclusion chromatography

Analytical size exclusion chromatography experiment was performed using Superdex 200 Increase 10/300 GL column (GE Healthcare) and ÄKTA purifier. The column was equilibrated with buffer containing 25 mM Tris pH 8, 250 mM NaCl, 5% glycerol and 10 mM $MgCl_2$. 500 μg of phosphorylated and non-phosphorylated $FleR_{FL}$, $FleR_{S150F}$ and $FleR_{R146E}$ were injected (100 μl). For phosphorylation, the proteins were incubated with 30 mM AcP on ice for 1 hour prior to injection. Furthermore, phosphorylated $FleR_{S150F}$ was incubated for 1 hour with 1 mM ADP alone and separately with 1 mM ADP, 5 mM NaF, and 0.8 mM $AlCl_3$ and subjected to size exclusion chromatography. UV absorbance at 280nm was recorded and the chromatograms were plotted in excel.

Small angle X-ray scattering (SAXS)

Small angle X-ray scattering (SAXS) data were collected for non-phosphorylated $FleR_{D53A}$ and phosphorylated $FleR_{S150F}$ and also for non-phosphorylated $FleR_{REC}$ domain at the BM29 BioSAXS beamline of ESRF, France. The experiment was performed at 10°C with a concentration of 8 mg/ml, 6 mg/ml and 4 mg/ml for $FleR_{D53A}$, 10 mg/ml, 5mg/ml and 2.5 mg/ml for $FleR_{REC}$ and 6 mg/ml, 4 mg/ml and 2 mg/ml for $FleR_{S150F}$. The proteins were in buffer containing 25 mM Tris pH 8, 300 mM NaCl, 5% glycerol and 2 mM DTT. 10 frames were collected for each sample and buffer with an exposure of 1 second per frame. PRIMUS (ATSAS 3.0.4 software package) and BioXTAS RAW software were used for data scaling, averaging (5, 4 and 3 frames were used for $FleR_{REC}$, $FleR_{D53A}$ and $FleR_{S150F}$, respectively) and buffer subtraction.[53,54] *Ab initio* bead model was generated using DAMMIF.[55] Seven-fold symmetry was applied for the phosphorylated $FleR_{S150F}$ data set to generate the bead model.

Structures of individual domains of FleR, were predicted using AlphaFold2[56] which were placed in the SAXS envelop as described in the results section in detail to obtain the inital model. The χ^2 values was calculated for the initial model with the experimental SAXS data using CRYSOL 2.0 and CRYSOL 3.0 for non-phosphorylated and phosphorylated data respectively.[57,58] To improve the χ^2 value, the initial model was subjected to flexible refinement with SREFLEX of ATSAS software.[59] The model with lowest χ^2 was superimposed on the SAXS envelop using SITUS (https://situs.biomachina.org/).

Dynamic light scattering (DLS)

Dynamic light scattering experiment was performed to analyse the size distribution of the protein in phosphorylated and non-phosphorylated state by Malvern Zetasizer Nano ZS instrument. The experiment was performed by using 0.1 mM protein in buffer containing 25 mM Tris pH 8.0, 250 mM NaCl, 5% glycerol and 2 mM DTT at 14°C with an angle of 90°. The protein was incubated with 40 mM acetyl phosphate and 10 mM $MgCl_2$ for 30 min at 4°C for phosphorylation. Additionally, phosphorylated $FleR_{S150F}$ was incubated for 1 hour with 1 mM ADP, 1 mM ATPγS alone and separately with 1 mM ADP, 5 mM NaF, and 0.8 mM $AlCl_3$. All the samples were centrifuged at 15000 rpm for 1hr before the experiment. Sixty readings were performed with 10 sec time span of each measurement. The size distribution data obtained from the Zetasizer software were plotted in Excel. All the experiments were performed in triplicates to calculate the standard deviations.

Negative staining of protein and visualization in TEM

Oligomeric form of phosphorylated $FleR_{S150F}$ was used for negative staining. Five microliter of protein samples (0.05 mg/ml of $FleR_{S150F}$ with 100 μM of ADP) were applied directly onto glow-discharged carbon coated grids (300 mesh size) for 40 sec. The grids were then blot dried and negatively stained with 2% uranyl acetate. The grids were examined on JEM-2200FS electron microscope operating at 200 kV and images were taken at a nominal magnification of 30000 X (ATPC, RCB). The micrographs of $FleR_{S150F}$ were processed in cryoSPARC v4.1.[42] Initially few particles were picked which were used as template for further particle picking. 2D class average was performed, good 2D classes were selected and 3D model was generated.

Transmission electron microscopy of bacteria

mPAO1, Δ$fleR_{FL}$ and complemented ($fleR_{FL}$, $fleR_{R146E}$, $fleR_{S150F}$, $fleR_{D53A}$) strains of *P. aeruginosa* were negatively stained by placing 5μl of sample onto the glow-discharged carbon coated grid (200 mesh size) for 5 min and stained with 2% aqueous solution of phosphotungstic acid. Images were taken at a magnification of 20,000 X on JEM-1400Flash. The bacterial samples used for negative staining were grown at 37°C in LB media till OD_{600} reach 0.8. LB media was supplemented with arabinose for growth of complemented strains.

In-solution chemical cross-linking

For detection of oligomeric state of $FleR_{REC}$, $FleR_{DBD}$ and $FleR_{AAA+}$ in solution, the proteins were chemically cross-linked with EGS (Ethylene glycol bis (succinimidyl succinate)) (sigma cat. No. 803219) in a buffer containing 25 mM HEPES pH 8.0 and 500 mM NaCl. For crosslinking 20 μM of $FleR_{REC}$, $FleR_{DBD}$ and 10 μM $FleR_{AAA+}$ was incubated with 1 mM of EGS for 10 min at room temperature. The reactions were stopped by adding SDS PAGE loading dye followed by heating at 95°C for 10 min. Samples were resolved on SDS PAGE and analysed by silver staining.

Motility assay

The motility assay for $fleR_{FL}$ knockout and complemented (pHERD20T-$fleR_{FL}$, $fleR_{AAA+DBD}$, $fleR_{AAA+DBD(S150F)}$, $fleR_{R146E}$, $fleR_{D53A}$ and $fleR_{S150F}$) strains of *P. aeruginosa* (mPAO1) was performed as previously described by Banerjee et al. 2019 with slight modification.[18] For swimming

motility assay, 0.3% soft agar was supplemented with 0.1% (w/v) arabinose. Standard deviations were calculated from three independent experiments.

RNA extraction and quantitative real-time PCR (qRT PCR)

mPAO1, *ΔfleR*$_{FL}$ (procured from Manoil Lab, University of Washington) and complemented (*fleR*$_{FL}$, *FleR*$_{D53A}$ and *fleR*$_{AAA+DBD}$) strains of *P. aeruginosa* were grown overnight in LB medium. Secondary cultures were set up and allowed to grow till OD_{600} reached 0.6 to 0.8 for total RNA extraction. LB media was supplemented with 0.1% arabinose for growth of complemented strains. Double volume of bacterial RNA protect solution (Qiagen) was added to the cultures (5ml) and centrifuged at 6000 rpm to pellet down the cells. Cell pellets were resuspended in 1 ml of Trizol (Invitrogen) and lysed by vortexing. RNA was extracted and purified using the RNeasy® Mini kit (Qiagen). Quantitative real-time PCR was performed using SuperScript III Platinum SYBR Green One-Step qRT-PCR Kit (Invitrogen). The *rpoD* gene (σ^{70}) gene was used as the reference. The relative levels of *flgB* and *flgF* gene expression was calculated by comparing with the reference gene. Standard deviations were calculated from two independent experiments.

QUANTIFICATION AND STATISTICAL ANALYSIS

Statistical details of the experiments (including statistical tests and number of replicates), where applicable, can be found in figure legends.